https://doi.org/10.5194/egusphere-2025-148
Preprint. Discussion started: 4 March 2025
© Author(s) 2025. CC BY 4.0 License.

Surface Ozone: Seasonal cycles, trends and events, a new perspective from the OPE station in France over the 2012 - 2023 period

Sébastien Conil[1], Gilles Bergametti[2], Laurent Langrene[1], Morgan Lopez[5], Olivier Masson[3], Cyril Pallares[4], Michel Ramonet[5]

[1]DISTEC/EES/OPE, Andra, Bure,55290, FRANCE
[2] LISA (Laboratoire Interuniversitaire des Systèmes Atmosphériques), Université Paris Cité and University Paris-Est-Creteil, CNRS, Paris, France,
[3] Institut de Radioprotection et de Sûreté Nucléaire (IRSN/PSE-ENV/SERPEN/LEREN), 13115 Saint Paul Lez Durance, France
[4] Atmo Grand Est, France
[5] Laboratoire des Sciences du Climat et de l'Environnement (LSCE), IPSL, CEA-CNRS-UVSQ, Université Paris-Saclay, Gif-sur-Yvette, France

Correspondence to: Sébastien Conil (sebastien.conil@andra.fr)

Abstract.

A comprehensive atmospheric dataset including hourly meteorological parameters, pollutants and methane mixing ratio and weekly beryllium-7 and sodium-22 activity concentration measured at the Observatoire Pérenne de l'Environnement (OPE) station from 2012 to 2023 was used to assess the interannual and intraseasonal variability of ozone. Weekly parameters were computed to characterize mean afternoon, mean nighttime, baseline and peak events for ozone as well as for NO_X, CO, CH_4. The mean afternoon O_3 concentrations did not show a significant trend, while baseline O_3 exhibited a significant increase of 0.7 µg.m^{-3} per year. The intra-seasonal variability of surface weekly ozone anomalies revealed two different periods. During the November to February period, ozone anomalies were related to CO, CH_4 and NOx anomalies but not with meteorological parameters or Stratosphere to Troposphere Transport (STT) proxies. From April to September, the relations between CH_4, CO and NO_X diminished while stronger association of O_3 residuals were observed with STT proxies, but also with temperature, solar radiation and relative humidity. The surface O_3 enhancement associated with positive anomalies of ^{7}Be and ^{22}Na suggests a direct stratospheric O_3 contribution but also a local photochemical contribution which is favored by warmer and drier air masses and increased solar radiations.

1 Introduction

In the stratosphere, ozone is beneficial to life on Earth thanks to the absorption of solar UV radiation. Conversely, it is usually a burden in the lower troposphere where it has significant health (e.g., Achebak et al., 2024, Fleming et al., 2018) and ecosystem impacts (e.g., Krupa and Manning, 1988, Lefohn et al., 1988, Cheesman et al., 2024) and acts as an additional greenhouse gas (IPCC, 2021). The main dynamic and chemical processes controlling its production and lifetime have been widely studied both in the stratosphere (Farman et al., 1985, Solomon 1999) and in the troposphere (e.g., Bell et al., 2005, Mills, et al., 2011). In the stratosphere, O_3 is formed by recombination of di-oxygen and an oxygen atom, resulting from the O_2 photolysis under UV radiations (< 320 nm). In the troposphere, O_3 formation is due to the nitrogen dioxide (NO_2) photolysis leading to NO + $O^{\cdot}$ and then the recombination of the atomic oxygen with O_2. However, a net production of O_3 implies that nitrogen monoxide reacts primarily with a hydroperoxyl radical (HO_2) to regenerate NO_2. rather than with O_3. These HO_2 radicals are produced by the oxidation of CO, CH_4 or Volative Organic Carbon (VOC) as those emitted by the vegetation or human activities. Because the tropospheric ozone production relies on the relative concentrations of nitrogen oxides and hydrocarbons, these compounds are often mentioned as precursors of the tropospheric ozone. The stratosphere constitutes another significant source of tropospheric ozone through the cross-tropopause downward transport of ozone enriched air masses.

https://doi.org/10.5194/egusphere-2025-148
Preprint. Discussion started: 4 March 2025
© Author(s) 2025. CC BY 4.0 License.

Intense efforts to implement networks monitoring the ozone concentrations from the surface to the stratosphere, using both in situ measurements and remote sensing techniques, have been deployed and maintained thanks to several global or regional initiatives such as European Monitoring and Evaluation Programme (EMEP), Network for the Detection of Atmospheric Composition Changes (NDACC), Southern Hemisphere ADditional OZonesondes (SHADOZ), In-service Aircraft for a Global Observing System (IAGOS) or in the framework of the International Global Atmospheric Chemistry Project (IGAC). In addition to these monitoring networks, many process studies and modeling developments have been supported in order to tackle global and regional issues and assess both their causes and origins. The main objective was to offer tools to help policy makers to propose solutions, implement actions and then evaluate their efficiencies (UNEP Montreal protocol, 1987, EU Air Quality Directive, US Clean Air Act, Long-Range Transport of Air Pollution Convention, 2015, China National Ambient Air Quality Standards 2012). An additional aim of these modeling developments was to attempt predicting the future changes in ozone concentrations from daily to decadal timescales in response to different climate change scenarios (e.g., Shen and Mickley, 2017; Young et al., 2018; Archibald et al., 2020; Bowman et al., 2022).

Benefitting from both observations and modelling historical efforts, five key dominant processes / parameters have been identified as major drivers of the tropospheric ozone concentrations (e.g., Monks et al., 2015): global ozone background, local photochemical processes (production and destruction), dry deposition, regional transport and stratosphere-troposphere exchange. Lightning NO_x, NO_x emissions from the soil, and ozone input from the stratosphere control the ozone background at a global scale. Obviously, the meteorological conditions and synoptic situations have significant influences on the relative contributions of each of these processes to the ozone background (e.g., Lu et al., 2019, Nguyen et al., 2022, Otero et al., 2016). The atmospheric chemistry of ozone production and destruction is complex and several regimes of O_3 chemistry have been identified according to its precursors relations. The non-linearity of the O_3–VOC–NOx reactions system led to the identification of a VOC limited and a NOx limited regime. The VOC-limited regime implies that the O_3 production is limited by VOC concentrations, meaning that an increase in VOC concentrations (while keeping NOx concentrations constant) will increase the O_3 production. Furthermore, in the presence of high NO concentrations, O_3 concentration values can become very low through titration (excess amounts of NO react with O_3 to form NO_2). This occurs quite frequently in the centers of urban areas; most megacities being classified as VOC limited and titration regimes. While some European regions were consistently either VOC sensitive or NOx sensitive, other areas experienced frequent changes of their regimes on a monthly or daily timescale, e.g., O_3 production could be limited by either NOx or VOC availability (Beekmann and Vautard, 2010)

Recent papers on surface concentrations or tropospheric column of O_3 observations gave contrasting results regarding regional trends and annual cycles. Compared to its preindustrial level, the global tropospheric ozone burden has increased by 45% mostly because of the increase of the anthropogenic precursor emissions (e.g., Parrish et al., 2012, Cooper et al., 2014; Archibald et al., 2020; Szopa et al., 2021; Wang et al., 2022; Fiore et al., 2022). A large share of this increase is taken by the tropical region (e.g., Gaudel et al., 2024) due to the ongoing shift of ozone precursor emissions from the mid-latitude regions toward the Equator. The largest increases in surface ozone in recent decades have been observed in eastern Asia (Ziemke et al., 2019; Lin et al., 2017) where high tropospheric ozone levels have been frequently observed (e.g., Fishman et al., 1990; Fishman et al., 1996; Logan et al., 1999; Ziemke et al., 2019). Over Europe, during the 1995–2014 period, a decrease in both the ozone peak (i.e., the 95th percentile of the ozone concentration distribution) and the mean values was observed at surface EMEP sites while the background (defined as the 5th percentile ozone concentrations) still increased (Yan et al., 2018). The mean surface ozone trend estimates also depend on the timeframe considered (e.g. a global increase since the 1970s contrasting with recent decrease since 2000) (Gaudel et al., 2018, Cooper et al., 2020). In addition, large variations are often observed between regions but also between local stations within a region (Archibald et al., 2020; Sicard, 2021; Massagué et al., 2023).

https://doi.org/10.5194/egusphere-2025-148
Preprint. Discussion started: 4 March 2025
© Author(s) 2025. CC BY 4.0 License.

Tropical regions showed different patterns compared to extratropical regions while the USA and Europe contrasted with Asia and China. Moreover, ozone peaks have experienced different trends as compared with the lower percentile background values or mean concentrations (Diaz et al., 2020, Gaudel et al., 2020).

Ozone is a major issue around cities because it is produced by urban emissions of precursors which photochemically react in the plume during its transport to surrounding suburban areas. Since the 1990s, background ozone concentrations have increased more slowly due to the reductions in emissions of the ozone precursors (e.g. Vautard et al., 2006, Monks et al., 2009). Changes over the USA and Europe since the 1990s are characterized by contrasted decrease in summertime peaks and increase of the annual ozone mean concentration (Gaudel et al., 2018). Shifts in the magnitude of the ozone seasonal cycle (Bowman et al., 2022) or timing (Parish et al., 2013) were also observed in these northern midlatitudes regions.

Thus, the ozone concentration at any location can be interpreted as a combination of a baseline, an advected component and a local photochemical production. The long-range contribution to the ozone baseline is largest in spring and weakest in summer (Fiore et al., 2009). Recent analyses of long-term trends in baseline ozone in western regions of North America (Parrish et al., 2017) and Europe (Derwent et al., 2018) have shown increasing trends from the beginning of the first reliable measurements in the 1980s until approximately 2000–2010. They also indicate that these trends may begin to slow down and possibly reverse. But McHugh et al. (2023) reported significant long-term (2005–2019) increases in annual O_3 concentration at two Irish rural stations. The local and regional precursors emissions may have only a minor influence on the annual average of surface ozone compared to extra-regional emissions of both NO_x and reactive carbon (Butler et al., 2020). In this study, methane, as a long-lived precursor, contributed to 35 % of the tropospheric ozone burden and 41 % of the northern hemisphere 2010 annual average surface ozone concentration.

The transport of air from the stratosphere to the troposphere (STT) is also a significant contributor to surface ozone concentrations as the stratosphere is the main ozone production zone (e.g., Archibald et al., 2020; Stohl et al.,2003). The stratosphere being dryer than the troposphere, these STT are often associated with a drying of the tropospheric layers affected by such downdrafts. This transport occurs during specific atmospheric synoptic situations favoring tropopause folds, stratospheric air intrusions and gravity wave breaking (Stohl et al.,2003). The timing, the horizontal and vertical scales of these atmospheric phenomena make direct observations difficult (e.g., Kuang et al., 2017, Luo et al., 2024). To cope with these difficulties, many studies rely on the use of models (e.g., Akritidis et al., 2016, Skerlak et al., 2019, Zanis et al., 2014, Wang and Fu, 2021, Ruiz and Prather, 2022) or dynamical/chemical tracers (e.g., Putero et al., 2016, Kalabokas et al., 2020, Trickl et al., 2023, Trisolino et al., 2024) to try to quantify the O_3 transfers from the stratosphere.

Looking for a stratospheric ozone proxy, cosmogenic radionuclides such as Beryllium-7 (^{7}Be) and Sodium-22 (^{22}Na) can be used as STT tracers even if there exist several limitations as pointed out by Terzi et al. (2020). Indeed, ^{7}Be is produced by the spallation of oxygen and nitrogen due to cosmic radiation in the upper troposphere and lower stratosphere regions (Stohl et al., 2003). Similarly, ^{22}Na stems from the interaction of cosmic radiation with argon in the upper atmosphere. Once produced, cosmogenic radionuclides attach to aerosols and are then transported by the atmospheric circulation. Their stratospheric concentrations are one to two orders of magnitude higher than corresponding tropospheric values (Luyanas et al., 1970). Apart from the production rate whose variations are closely linked to the solar activity cycle and O, N, Ar gas concentrations, the variations of the ground-level ^{7}Be and ^{22}Na activity concentrations are related to atmospheric transport and to deposition processes. The ^{7}Be and ^{22}Na production zone includes the stratosphere (about 70%) but also the upper troposphere (about 30%). However, owing to their respective radioactive half-life (53.2 day for ^{7}Be and 2.603 year for ^{22}Na) they have different residence times in the atmosphere. Many authors have used ^{22}Na in addition to ^{7}Be through the ^{7}Be /^{22}Na ratio to identify STT events (e.g., Steinmann et al., 2013, Rodriguez-Perulero et al., 2019, Leppanen and Poluianov, 2022). As the production of ^{7}Be and ^{22}Na have different vertical profiles, the ^{22}Na /^{7}Be ratio can also be used as a signature of the vertical location of the

https://doi.org/10.5194/egusphere-2025-148
Preprint. Discussion started: 4 March 2025
© Author(s) 2025. CC BY 4.0 License.

air masses origin, the ratio increasing with increasing altitude (in the stratosphere). Apart from the altitude and thus the closeness to the production zone, the ^{7}Be spatial variations in Europe are mostly clustered by latitude, the northern Europe (50°N and above) having different mean levels and seasonal cycles compared to Western and Central Europe (Hernandez Ceballos et al., 2016, Ajtic et al., 2018). The latitudinal dependencies of ^{7}Be but also ^{22}Na and thus ^{22}Na/^{7}Be ratio was also noticed in Hoffmann et al. (2018) which related its signature to the global 2D atmospheric circulation. Maximum stratospheric fingerprints in the lower atmosphere are associated with the descending branch of the Hadley cells (Holton et al., 1995) and mean surface activities are decreasing from the mid latitudes to the polar regions. In addition, the mean residence time of the aerosols carrying the stratospheric radionuclides seems to be latitude dependent, from around 10 days in the midlatitudes to around 100 days in the polar regions, as underlined by Leppanen and Poluianov (2022).

The STT in the midlatitudes is associated with intermittent synoptic-scale and mesoscale processes controlling its time and space scales (Holton etal., 1995, Stohl et al., 2003). These intruding stratospheric air masses often forming filamentary structures are difficult to monitor on a regular and systematic basis but can be observed indirectly in various situations or during specific dedicated intensive field campaigns (e.g. Zanis et al., 2003; Langford et al., 2022; Chen et al., 2024). Their fingerprints are sometimes revealed by the potential vorticity, radioactivity levels, ozone or water vapor (Cristofanelli et al., 2006; Trisolino et al., 2024) but often need modeling efforts to be confirmed (Akriditis et al., 2018).

This work contributes to the scientific understanding of ozone interannual and intraseasonal variability using a consistent dataset of measurements performed at a continental regional background station, OPE, located in the north-eastern part of France, over the 2012-2023 period. We connect the changes in surface ozone concentrations at different time scales with several key parameters that are known to play a role in the ozone chemistry: chemical precursors CH_4, CO, NO_x, surface meteorological parameters (temperature, relative humidity, wind speed, rainfall, solar radiation) and stratosphere/upper troposphere associated tracers ^{7}Be and ^{22}Na.

2 Data and method

2.1 Site location

The Observatoire Pérenne de l'Environnement (OPE) atmospheric station (48.5625°N, 5.50575°E WGS84, 395 m asl) is located in the north-eastern part of France. The station sits in a rural area and is surrounded by large crop fields, some pastures and patches of forest (Fig. S1). The dominating land cover types according to Corine Land Cover 2012 in the 25 / 100 km surroundings are Arable land/crops: 39% /44%, Pastures: 14% /18%, Forest: 44% /34%. The mean population density within a 25/100 km radius from the station based on GEOFLA database from the Institut National de l'Information Géographique et Forestière (IGN) are 26/64 (inhab.km^{-2}). The closest villages are Delouze (130 inhabitants) located 1 km at the SE and Houdelaincourt (300 inhab.) located 2 km at the SW. The closest cities are Saint-Dizier (45,000 inhab.) located 40 km away to the west, Bar le Duc (35,000 inhab.) 30 km to the north-west, Toul (25,000 inhab.) 30 km to the east and Nancy (450,000 inhab.) 50 km to the east. The major road (RN4) with 20,000 cars day is located 15 km to the north. The station facilities include a 120 m tall tower and a 100 m^2 building hosting the samplers and analyzers.

2.2 Meteorology measurements

The key meteorological parameters are monitored using a ground-based weather station operated by Météo-France, the French national weather service providing hourly mean data in compliance with the World Meteorological Organization specifications. The following standard meteorological parameters are monitored: temperature, relative humidity, pressure, wind speed and direction, global solar radiation and rainfall. The mean annual temperature over the 2012-2023 period is about 10.8°C (with a standard deviation of 1°C). The minimum recorded temperature was -15.3°C and the maximum temperature

https://doi.org/10.5194/egusphere-2025-148
Preprint. Discussion started: 4 March 2025
© Author(s) 2025. CC BY 4.0 License.

was 39.1°C. The cumulated annual precipitation was on average 817 mm (with a standard deviation of 128 mm). Mean annual solar radiation was 420.7 kJ.cm^{-2} (with a standard deviation of 21 kJ.cm^{-2}) and the mean annual sunshine duration was 1828 hours (with a standard deviation of 250 hours). Two local wind regimes are prevailing: a south/westerly regime and an easterly/north-easterly regime.

The hourly Boundary Layer Height (BLH) data was extracted from the European Centre for Medium-Range Weather Forecasts (ECMWF) ERA5 reanalysis at the grid point closest to the station location using the Copernicus Climate Data Store (https://cds.climate.copernicus.eu/datasets/reanalysis-era5-single-levels)

2.3 Ozone, NOx, CH_4 and CO measurements

For O_3 and NO_x, the sampling system includes an inlet on the roof of the building approximately 4 m above the ground. From 2011 up to now ozone concentrations have been measured using a Thermo TEI49i (Thermo Scientific) UV analyzer. NO_x concentrations were reported using a Thermo TEI42i (Thermo Scientific) analyzer from 2011 to September 2020 and since with a Teledyne T200 UP analyzer. Quality checks, calibration, intercomparison and data processing are performed routinely according to the French Standard Operating Procedures (SOP), in agreement with the European Air Quality Directive and EMEP rules (Macé, 2016). Hourly data are reported in µg m^{-3}.

For both CH_4 and CO, the main sampling inlets are located at 10 m and 120 m above ground level (agl). CH_4 was measured using Picarro G1301, G2301 and G2401 analyzers. Several analyzers were used to report the CO concentrations: a Los Gatos DLT100 analyzer, a Picarro G2401 and a Picarro G5301. The quality checks, calibration, intercomparison and data processing are performed using the ICOS SOP (see Conil et al., 2019 for details). Hourly concentrations are reported on the WMO-CO-2014 scale in dry mole fraction ppmv for CO and on the WMOX2004A in dry mole fraction ppbv for CH_4. The station footprint and its representativity differ significantly between nighttime and afternoon due to the mixing layer daily cycle. Thus, 10m agl /120m agl data are used to compute respectively nighttime/afternoon statistics based on the assumption that the afternoon boundary layer is well mixed while stratification and residual layers may occur during the night implying a larger vertical gradient even in the first 100 m above the surface (Conil et al., 2019).

2.4 Radionuclide measurements and solar activity index

^{22}Na and ^{7}Be are cosmogenic radionuclides primarily produced in the stratosphere. They are transported to the troposphere and then follow the general atmospheric circulation (Delaygue et al., 2015, Terzi et al., 2020). To exceed detection limits and obtain a sufficient signal to noise ratio, it is necessary to combine an appropriate detection method and a sampling period long enough to accumulate sufficient particulate matter and activities (in Bq). This is particularly the case with ^{22}Na whose ground level activity concentration usually ranges between a few hundredths to one µBq m^{-3} while ^{7}Be varies between one thousand and ten thousand µBq m^{-3} which does not pose detection issue. Conversely, ^{22}Na is seldom determined and usually requires high-volume sampling and low-level measurement capabilities. This is usually achieved thanks to weekly sampling periods (Rodriguez-Perulero et al., 2019, Alegria et al., 2020, Hernandez Ceballos et al., 2022).

At the OPE station, the monitoring of these airborne radionuclides is routinely based on weekly sampling using a high-flowrate sampler (roughly 1,000 m^3·h^{-1}, Snow White aerosol sampler from Senya). This weekly sampling routine is modified when special events occur in order to increase the sampling frequency (see Masson et al., 2019 for example). The weekly samples collecting nearly 160,000 m^3 of ambient air on very high efficiency filter (one layer of polypropylene and electret media 3M 5379 BMF, 20 g m^{-2}) are pressed in a small pellet before measurement. The detections are then performed at the Institut de Radioprotection et de Sûreté Nucléaire (IRSN) metrology lab in Orsay (France) using a high-purity germanium (HPGe) gamma-ray spectrometer system. In addition, the sunspot number index was used as a proxy of the solar activity to evaluate the solar contribution to the stratospheric production of ^{7}Be and ^{22}Na. The sunspot number data were freely downloaded from the WDC-SILSO website (https://www.sidc.be/SILSO/home).

https://doi.org/10.5194/egusphere-2025-148
Preprint. Discussion started: 4 March 2025
© Author(s) 2025. CC BY 4.0 License.

2.5 Data processing

The data processing effort made extensive use of the R openair package from Carslaw and Ropkins (2012). From the hourly NOx, CH_4, CO and O_3 data nighttime means were computed from 00:00 to 04:59 UTC and afternoon means from 12:00 to 16:59 UTC, to represent the two contrasting periods of the day: nighttime without solar radiation, with decreasing temperatures and lower mixing layer and mid-afternoon with solar radiation, warmer temperature and higher mixing layer. We computed weekly average of the mean afternoon and mean nighttime data. We also used the weekly statistics of the hourly data to describe the median conditions, baseline levels (lower 5% percentile hereafter q5) and peak events (95% percentile hereafter q95). A visual illustration of the transformation from hourly data to weekly data is shown in Fig. S2 displaying hourly data over nine days around the week of May 2 to 9, 2022 along with the mean afternoon, mean nighttime, baseline concentration (q5) and peak concentration (q95) derived from the hourly data.

Using these weekly data, we estimated the mean seasonal cycle and performed a trend analysis using several complementary tools. We fit the weekly time series to separate functions for the average long-term change (LTC) and the superimposed seasonal cycle (SC): LTC(t) + SC(t). We used the CCGCRV curve fitting program (Thoning et al., 1989) with the standard parameters set to compute the mean seasonal cycles and trends. CCGCRV results were compared with similar analysis performed with the openair package of R for the seasonal cycle and the trend component using the Theilsen and STL methods (Pickers and Manning, 2015). The parameters set used for CCGCRV were: - short-term cut-off period (fs), 182 days, long-term cut-off period (fl), 1095 days, number of harmonic terms, 4 and degree of polynomial function, 3. The STL parameters set used was periodicity of the seasonal component: 12 months, span of the loess window of the low-pass filter 13 months, and the seasonal component were estimated as the mean. CCGCRV was preferred as it can process weekly data in a nonlinear framework. STL was used as a verification tool on monthly aggregates while the TheilSen method gave robust estimators (even for non-normal data) along with their confidence levels. These seasonal cycles and trend components of the time series are dominated by large-scale processes. Since we have a particular interest for the intra-seasonal atmospheric variability, we used the CCGCRV method to estimate the weekly residuals (hereafter mentioned as “anomalies” or “residuals”) by removing the seasonal cycle and long-term trend components from the weekly data. We then computed the correlation coefficients and displayed boxplots and scatterplots to assess relationships between ozone anomalies, temperature, solar radiation, relative humidity as meteorological drivers, ^{7}Be and ^{22}Na residuals as representatives of STT, and NO_x, CH_4 and CO as chemical precursors.

3 Results

3.1 Seasonal cycles

3.1.1 Ozone

The mean surface ozone concentrations at OPE was 63.6 µg m^{-3} (31.9 ppbv) over the 2012-2023 period. A mean O_3 concentrations of 53.7 µg m^{-3} was observed in Ireland during the 2015-2019 period at 11 stations, the highest mean being reported at the Mace Head (MHD) coastal station with 74.5 µg m^{-3} and the other rural stations reported between 50 and 58 µg m^{-3} (McHugh at al., 2023). The eastern Europe Polish rural station Belsk reported an annual mean surface concentration of 54.6 µg m^{-3} during the 2015-2023 period (Pawlak et al., 2024). Annual concentrations ranging from 40 to 80 µg m^{-3} were also observed in different regions of Portugal during the period 2012-2019 (Silva and Pires, 2022). EMEP rural stations had an average ozone concentration of around 70 µg m^{-3} over the 1995-2013 period, significantly higher than other suburban and urban European stations (Yan et al., 2018). A mean ozone concentration around 100 µg m^{-3} was reported at the two European mountain stations of Zugspitze (ZUG) and Jungfraujoch (JFJ) over the 2000-2010 period while the Irish coastal station of MHD and the Western German station of Hohenpeißenberg (HPB) showed similar levels at slightly below 80 µg m^{-3} (Cooper

https://doi.org/10.5194/egusphere-2025-148
Preprint. Discussion started: 4 March 2025
© Author(s) 2025. CC BY 4.0 License.

et al., 2014). The Italian mountain station of Monte Cimone (CMN) observed an even higher mean O_3 concentrations of 108 µg m^{-3} over the 1996 to 2011 period (Cristofanelli et al., 2015).

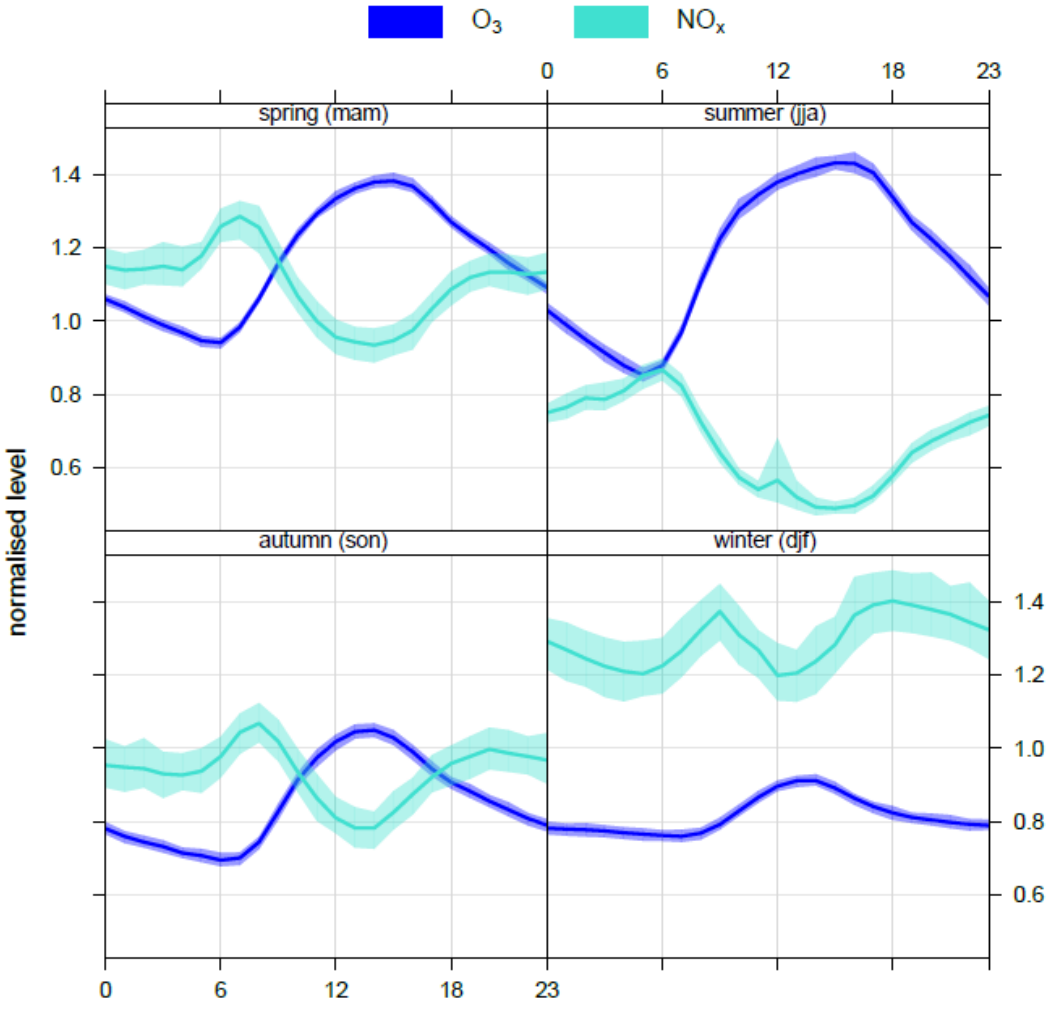

Figure 1: Normalized mean diurnal cycles of O_3 (blue) and NOx (cyan) over the four seasons from spring (upper left) to winter (bottom right) computed over the period 2012-2023 at OPE.

Figure 1 shows the NO_x and O_3 diurnal cycle over the spring to winter seasons. The NO_x hourly mean concentrations were characterized by two maxima, one occurring early in the morning (between 06:00 and 08:00 UTC) and the second appearing in late afternoon (between 17:00 and 19:00 UTC) and two minima during the night and the afternoon, the morning peak being the largest and the afternoon minimum, the lowest. O_3 concentrations showed an afternoon maximum and a late night/early morning minimum. Similar diurnal patterns have been observed at rural sites in Ireland (McHugh at al., 2023), Portugal (Silva and Pires, 2022) and Spain (Massagué et al., 2019, Hernandez Ceballos et al., 2022) over the recent years. The early morning NO_x peak is attributed to the NO increase associated with NO_2 destruction and O_3 production. The late afternoon secondary NO_x maximum is associated with the NO_2 increase while O_3 and NO decreased. The diurnal changes of CH_4, CO, air temperature, boundary layer height (BHL) (Fig. S3 to Fig. S7) followed a typical cycle with mid-afternoon maxima and late night/early morning minima while relative humidity showed the opposite variations.

https://doi.org/10.5194/egusphere-2025-148
Preprint. Discussion started: 4 March 2025
© Author(s) 2025. CC BY 4.0 License.

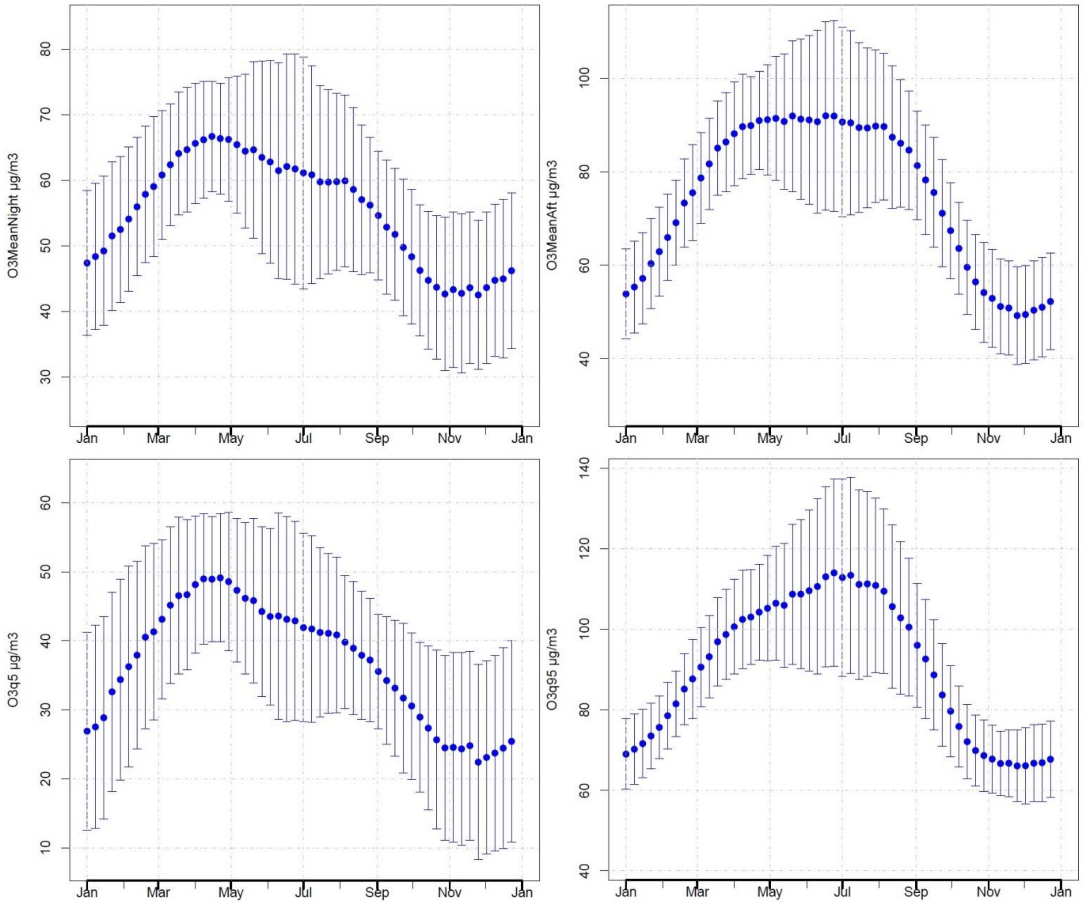

Figure 2: Averaged seasonal cycles of nighttime mean (00:00 to 04:59 UTC) O_3 (top left panel), afternoon mean (12:00 to 16:59 UTC) O_3 (top right panel), O_3 q5 (bottom left panel) and O_3 q95 (bottom right panel) and standard deviations for the period 2012-2023.

At OPE the mean annual cycle of monthly surface ozone concentrations showed a mostly linear increase from a lowest level in November around 45 µg m^{-3} (22.5ppbv) to a maximum in April around 77 µg m^{-3} (39ppbv) followed by a ridge of high levels around 75 µg m^{-3} (38ppbv) from May to July, and a fast decrease from August (around 71 µg m^{-3}) to October (around 51 µg m^{-3}) (Table S1 with monthly means and Fig. S8 with weekly means). A similar pattern was reported in Boletti et al. (2020) for a cluster of Western European stations with minimum level in November and December and a ridge extending from May to August. The JFJ mountain station also showed a similar annual cycle and the CMN station exhibited a peak in July while showing the same low levels in fall and winter (Cristofanelli et al., 2015). On the contrary, a seasonal pattern with a spring maximum and a summer–autumn minimum was observed at the Irish rural stations. This spring maximum was also reported at a cluster of northern European stations including Irish and British ones. Those annual cycle contrasting patterns were also noticed by Monks et al. (2015). The large maximum ridge over the spring/summer and the fall/winter minimum is a typical continental annual cycle (Gilge at al., 2010; Tarasova et al., 2007) differing from northern hemisphere remote sites where a spring maximum in April/May is usually observed (Monks, 2000; Tarasova et al., 2007). The observed broad spring/summer maximum is commonly interpreted as a combination of contributions from large scale transport of enhanced background with the addition of large photochemical production from regional emissions (e.g. Zanis et al., 2007; Monks et al., 2009).

Figure 2 shows the mean seasonal cycles of some O_3 indicators at the OPE station over the 2012-2023 period. The mean nighttime O_3 concentrations (upper left panel of Fig. 2) and the O_3 baseline (lower left panel of Fig.2) showed a similar pattern

https://doi.org/10.5194/egusphere-2025-148
Preprint. Discussion started: 4 March 2025
© Author(s) 2025. CC BY 4.0 License.

characterized by a marked sinusoidal cycle with a maximum in April at respectively 66 and 45 µg m^{-3} and a minimum in November at respectively 42 and 22 µg m^{-3}. The peak event (lower right panel of Fig.2) and mean afternoon (upper right panel of Fig. 2) concentrations also showed a marked annual cycle but with a minimum in early winter (Nov-Jan) at 66 and 49 µg m^{-3} respectively and a broad maximum in the warm period (May to September) above 110 and 90 µg m^{-3} respectively. Similar contrasts between the annual cycle of nighttime and afternoon mean O_3 concentrations were observed by Tarasova et al., 2007) over a region covering part of France and Germany and the Netherlands. The afternoon O_3 concentrations were larger than the nighttime concentrations, with an average difference of 20 µg m^{-3}, because of the large photochemical production. In general, maximum surface O_3 concentrations are observed when the boundary layer is larger (during the afternoon and in summer) because the photochemical production of O_3 is more important than its mixing in a larger volume induced by the increase in the boundary layer height and in vertical turbulent mixing.

3.1.2 NO_x, CO, CH_4

Figure 3 shows the mean seasonal cycles of NO_x, CO, CH_4, ^{7}Be, ^{22}Na, and of the $^{7}Be/^{22}Na$ activity ratio at OPE. The baseline, median and peak concentrations of NO_x, CO and CH_4 shared a similar seasonal pattern: a minimum in summer and a maximum in winter. Mean afternoon, nighttime and median NO_x decreased to low concentrations (≈ 5 µg.m^{-3}) from June to September and had maxima in January/February (≈ 10µ g m^{-3}). NO_x peak concentrations rose to their maximum from December to February, while the NO_x baseline reached its maximum in March and then decreased toward its minimum in early July. Similar seasonal NO_x cycles are commonly observed in Europe (Adame et al., 2022, Cristofanelli et al., 2021). However, the mean concentrations are quite different depending on the station type: expanding from low concentrations at mountaintop global station like HPB, JFJ (Gilge et al., 2010) or CMN (Cristofanelli et al., 2021) to high concentrations at urban stations (Massagué et al., 2019) while the rural background stations like OPE are in between. As already shown in Conil et al., (2019), the CO and CH_4 seasonal cycles exhibit minimum concentrations in July, at about 110 and 1,950 ppbv respectively, and then increased to reach two distinct maxima in November and in February, at about 180 and 2,000 ppbv respectively. While the CH_4 year-to-year variability looked quite stable all year long, the CO variability was much larger during the cold period with a relative standard deviation below 10% than during the warm period with a relative standard deviation of nearly 25%.

3.1.3 7Be, 22Na, and the 7Be/22Na ratio

The annual cycle of ^{7}Be and ^{22}Na activity concentrations had a similar pattern (Figure 3) falling for ^{7}Be toward a minimum at 2,080 mBq m^{-3} during late fall/early winter and growing back to maxima during spring and summer above 4,700 mBq m^{-3}. The ^{22}Na maximum at 0.6 mBq m^{-3} was reached in May and June while ^{7}Be showed a rather broader maximum activity from May to August. Similar seasonal cycles were also observed in several parts of Europe (Bourcier et al., 2011, Steinman et al, 2013, Hernandez Ceballos et al., 2015, Baray et al., 2017, Rodríguez-Perulero et al., 2019). However, the warm months ^{7}Be maxima is much more widespread, with high activity levels extending from May to August, that the one observed at the northern European stations. The maximum activity period was also associated with larger year-to-year variability while the cold period with lower activity showed smaller variability but a larger relative standard deviation.

The ^{7}Be and ^{22}Na mean activities and variability in the troposphere are largely associated with STT but not in an unambiguous way. In fact, the change in their tropospheric activity stems from variations in the multi solar activity cycles (yearly, 11-year, 80-year) and associated production rates, or by changes in the carrier aerosol life cycle (wet deposition for example). Similar seasonal cycles were observed in France (Baray et al., 2017), Switzerland (Steinmann et al., 2013), Poland (Blazej and Mietelski, 2014) or in Finland (Leppänen and Poluianov, 2022).

https://doi.org/10.5194/egusphere-2025-148
Preprint. Discussion started: 4 March 2025
© Author(s) 2025. CC BY 4.0 License.

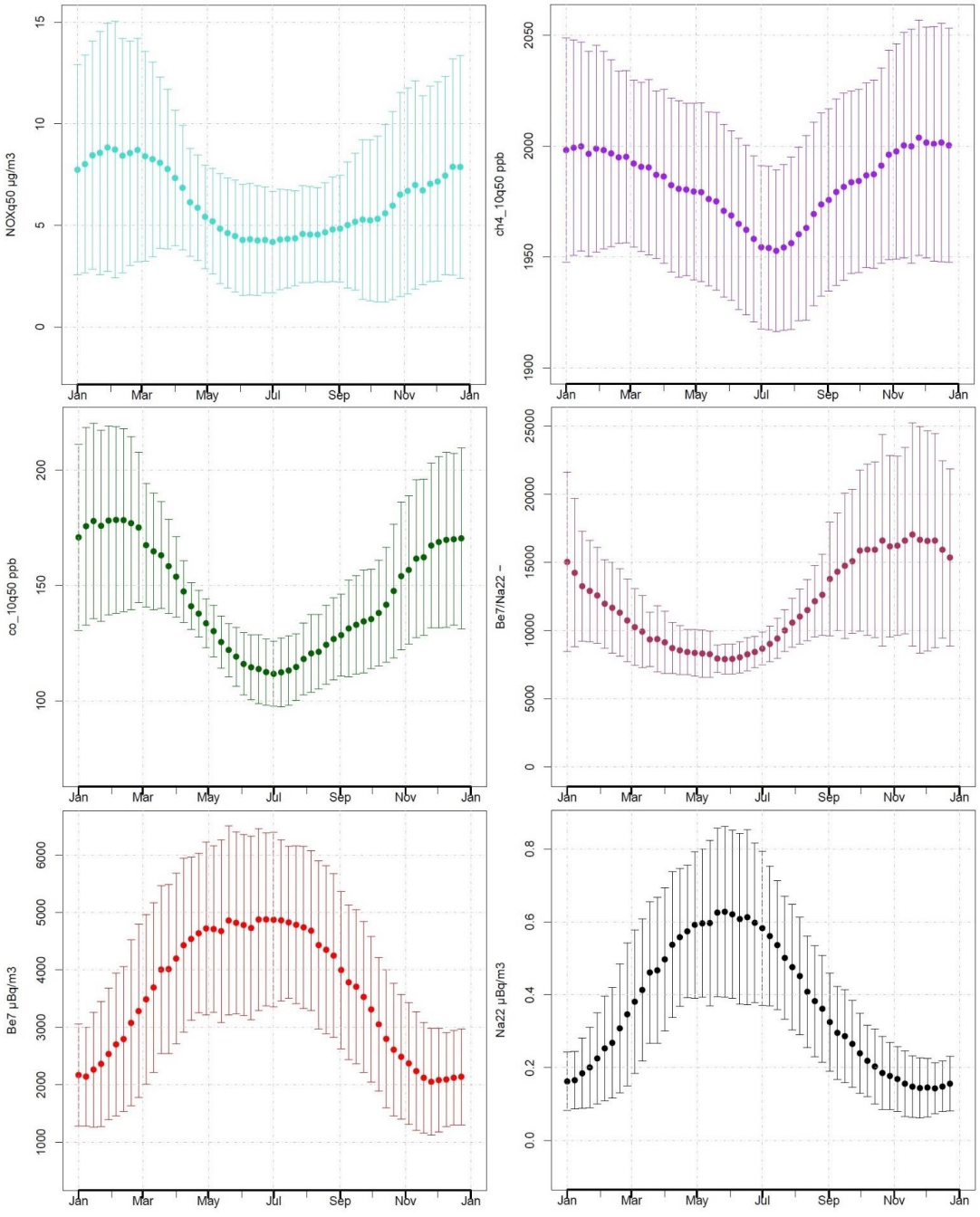

Figure 3: Averaged seasonal cycles of weekly median NO_x (top left panel), median CH_4 (top right panel), median CO (middle left panel), $^{7}Be/^{22}Na$ ratio (middle right panel), ^{7}Be (bottom left panel) and ^{22}Na (bottom right panel) and standard deviations for the period 2012-2023

The mean activity levels of ^{7}Be are strongly linked to the latitudinal position, as ^{7}Be concentration peak in the mid-latitudes and decrease toward the equator and poles. Higher number of STT events and upper troposphere downdrafts associated with anticyclonic situations, as well as weaker deposition during drier conditions may explain the increase of ground-level ^{7}Be

https://doi.org/10.5194/egusphere-2025-148
Preprint. Discussion started: 4 March 2025
© Author(s) 2025. CC BY 4.0 License.

activities during the warm period. The ratio ^{7}Be /^{22}Na (Figure 3) dropped down to a minimum of nearly 8,000 in late May/early June, May and June being associated with a rather low variability. Then it rose back to reach a level around 15,000 to 17,000 between October and early/mid-December, this period being characterized by a high variability of the ^{7}Be/^{22}Na ratio. This suggests that the STT is stronger in late spring and early summer and well reproducible from year to year while in late summer there are yearly changes of the STT intensity and frequency, some years having larger STT marked by lower ^{7}Be /^{22}Na ratio, and some others showing an increase in upper troposphere to lower troposphere transport marked by a higher ^{7}Be /^{22}Na ratio. The seasonal variations of the ^{7}Be and ^{22}Na activities together with the ^{7}Be/^{22}Na ratio reveal that while the stratosphere-troposphere transport is larger between March and August, the upper tropospheric air transport to the lower atmosphere is more active from June to August, while there is less transport from the upper to the lower troposphere during fall and winter. The increase of ^{7}Be/^{22}Na ratio in July suggests that STT event were still occurring but along with a strong upper tropospheric component (adding a ^{7}Be downward transport component but no additional ^{22}Na as its upper tropospheric share is much smaller).

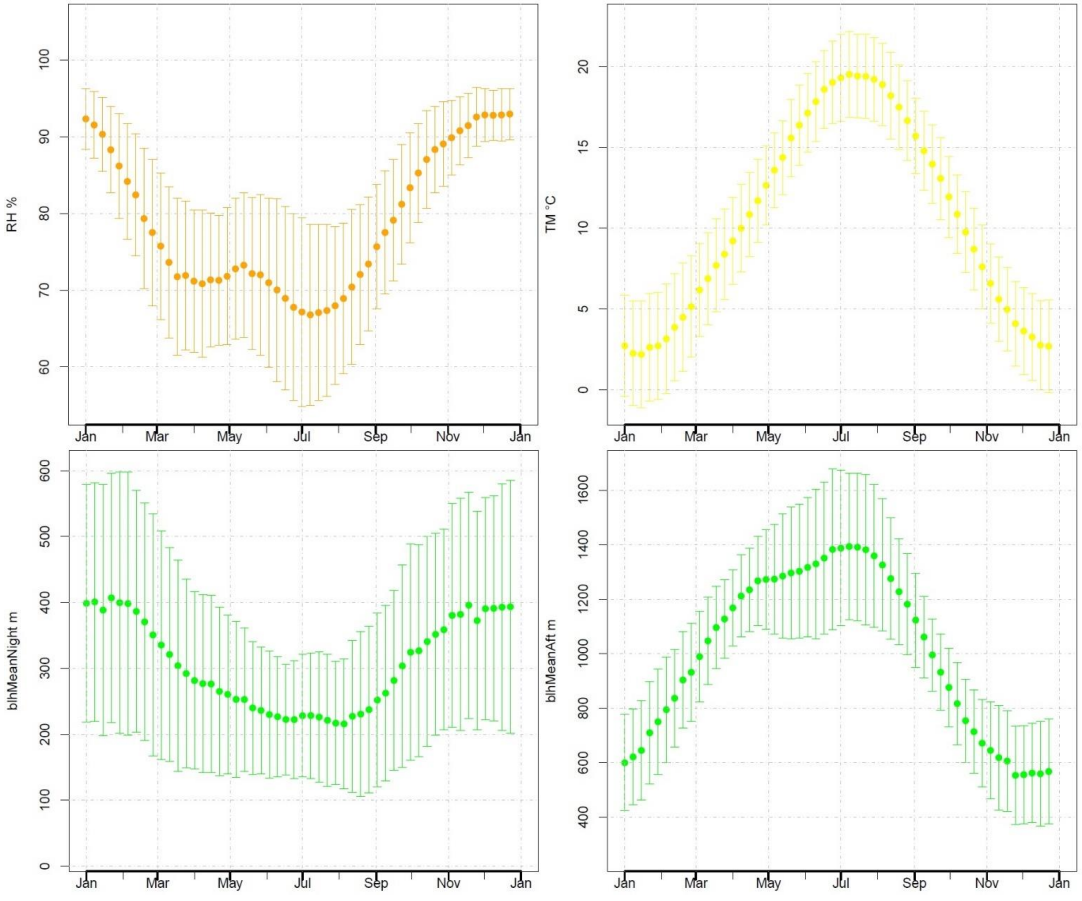

Figure 4: Averaged seasonal cycles of weekly mean relative humidity (top left panel), temperature (top right panel), nighttime mean (00:00 to 04:59 UTC) BLH from ERA5 (bottom left panel) and afternoon mean (12:00 to 16:59 UTC) BLH (bottom right panel) and standard deviations for the period 2012-2023

The relative humidity mean annual cycle (Figure 4) exhibits a specific cycle with minimum levels in summer (July/August) and spring (April) but maximum levels in fall and winter. The precipitations had a rather weak seasonal (not shown) cycle

https://doi.org/10.5194/egusphere-2025-148
Preprint. Discussion started: 4 March 2025
© Author(s) 2025. CC BY 4.0 License.

with minimum rates of about 12 mm per week in March and August and larger rainfall in fall and winter (above 20 mm per week) compared to its variability which was much larger than the mean annual cycle.

3.1.4 Peak Ozone and STT Events

At OPE, higher O_3 concentrations are experienced on average during daytime and over the spring to summer months while CO, CH_4 and NO_X concentrations reached higher levels during nighttime and wintertime. The O_3 baseline and peak events showed two distinct patterns, the former reaching its highest value in April while the latter peaked in July. STT and upper troposphere influence are stronger from May to August, the upper troposphere component increasing during that period as reflected by the decreasing ^{7}Be /^{22}Na ratio. These annual cycles are also reflected in the extreme event frequency distribution. Figure 5 shows the number of events associated with mean afternoon O_3 peak events (above 100 µg m^{-3} in blue and 130 µg m^{-3} in cyan) and STT events (^{7}Be above 4,200 µBq m^{-3}, in red and the ratio ^{7}Be /^{22}Na below 9,000 in black) aggregated per week over the 2012-2023 period. Events above the WMO air quality objective of 100 µg m^{-3} occurred from April to end of August with 20 to 30 events observed per week over the 11 years period meaning an average of 2 to 3 events per week. More intense event above 130 µg m^{-3} were observed in April and then in June and July with a frequency of 0.5 to 1 event per week on average. Large ^{7}Be activity concentrations also occurred from April to end of August, but the lowest ^{7}Be /^{22}Na ratio events were observed from mid-march to beginning of July. These frequency event distributions suggest that very large ozone events are associated with STT but not in a systematic and linear way. In May, the STT events are associated with O_3 events but not very large event while in June-July the very large O_3 events seem related with upper troposphere and STT events.

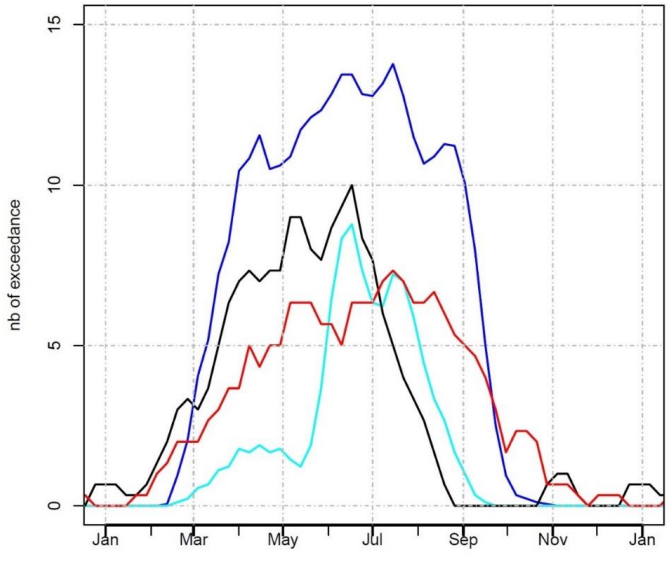

Figure 5: Number of exceedance day per week aggregated over the 2012-2023 period associated with afternoon mean (12:00 to 16:59 UTC) O_3 above two different thresholds (100 µg m^{-3} in blue, numbers divided by two and 130 µg m^{-3} in cyan), ^{7}Be activities above 4200 µBq m^{-3},in red and the ratio ^{7}Be /^{22}Na below 9000 in black. A 3 weeks rolling mean filter was applied to smooth the seasonal cycle.

3.2 Trend and interannual variability

The trends in the different O_3 time series representing baseline, median and peak event and nighttime and afternoon means over the 2012-2023 period showed similar inter-annual patterns (Figure 6). The nighttime mean and baseline O_3 experienced a significant increase respectively of 0.38 and 0.71 µg m^{-3} yr^{-1}, on which a decadal cycle was added with relatively higher values from 2018 to 2020 and lower values from 2015 to 2017 and in 2021. The mean afternoon and peak event concentrations did not experience any significant linear trend but showed similar decadal variation patterns. While O_3 trends do not show a

https://doi.org/10.5194/egusphere-2025-148
Preprint. Discussion started: 4 March 2025
© Author(s) 2025. CC BY 4.0 License.

consistent pattern across Europe (Boleti et al., 2020), similar contrasting trends with decreasing mean and maximum concentrations and increasing baseline concentrations were recently observed in the UK (Diaz et al., 2020), Ireland (Mc Hugh et al., 2023), Poland (Pawlak et al., 2024), Spain (Massagué et al., 2024a). However, one should emphasize that the inter-annual variability is much larger than the trend magnitudes (whatever the sign of the trend) meaning that a change in the timeframe of the analysis would change the trend estimates for the different ozone parameters either mean/median values, peak levels or baseline.

Over the 2012-2023 period, the mean air temperature showed a significant increase of 0.13°C yr^{-1}. The minimum and maximum temperature also showed an increase but with only marginal significance. On top of this linear increase the temperature experienced some interannual variations as shown by the CCGCRV second degree polynomial trend estimate (Figure 7). On average, periods with warmer / cooler temperature were associated with higher/lower ozone surface concentrations, respectively. The solar radiation showed a slight increase associated both with an increase in the sunshine duration and in the solar activity. Precipitation did not show any significant trend contrasting with a slight decrease of the relative humidity.

Over the 2012-2023 period, ^{7}Be and ^{22}Na surface concentrations trends (Figure 6) clearly reflected the 11-year solar activity cycle that is evidenced by the sunspot number index from SILO. Indeed, the sunspot number changes are anti-correlated with the 11-year variation of the cosmic ray intensity (Singh et al., 2017) and thus with the production of ^{7}Be and ^{22}Na. At OPE, minimum ^{7}Be and ^{22}Na surface activity concentrations were observed from 2014 to 2016 and in 2023. Maximum surface ^{7}Be and ^{22}Na surface activity concentrations were observed in 2012 and from 2017 to 2022.

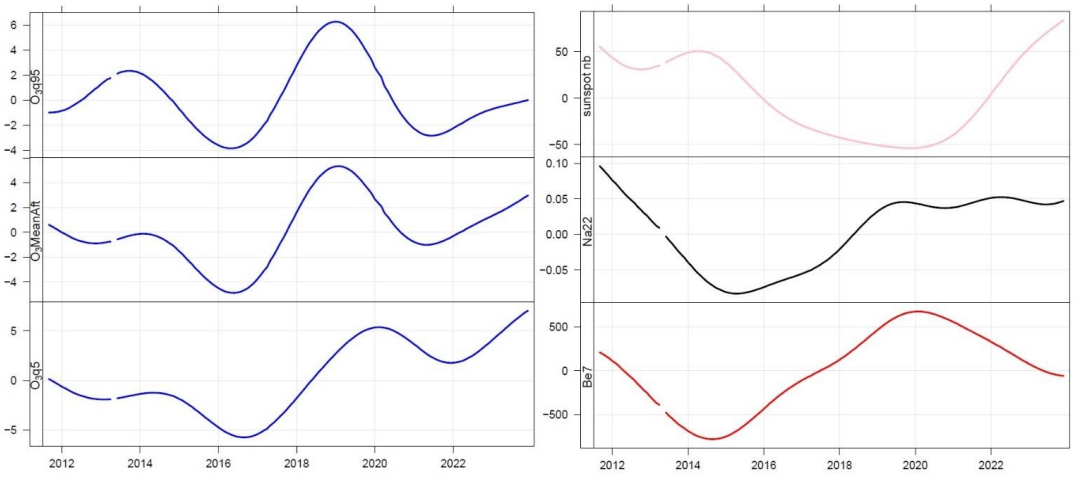

Figure 6: Long-term trends computed with CCCGRV using weekly deseasonalized O_3 (blue) peak event (q95 upper left panel, µg m^{-3}) mean afternoon (12:00 to 16:59 UTC, middle left panel, µg m^{-3}), baseline (q5 bottom left panel, µg m^{-3}) and sunspot number index (pink, upper right panel), ^{22}Na activities (black, middle right panel, µBq m^{-3}) and ^{7}Be activities (red, bottom right panel, µBq m^{-3}) computed over the period 2012-2023 at OPE.

The different NO_x and CO parameters (baseline q5, median q50 and peak events q95 as well as their afternoon and nighttime means) showed significant decrease (Figure 7), the peak intensity decrease being the largest (compared to mean and baseline). Recently, similar decreasing trends were observed in Spain and Italy (Cristofanelli et al., 2021, Adame et al., 2022). These decreases are related to the main anthropogenic emission reduction over Western Europe associated with stronger environmental protection policies such as the EU clean air directive.

On the other hand, over the same period CH_4 concentrations experienced large increases as observed at different stations for several years. Its causes, which are still stiffly debated, may include an increase of the anthropogenic emissions, as well as the emissions from tropical wetlands which also contribute to high growth rates between 2020 and 2022 (Lin et al., 2024). It may also be partly related to decreases in OH radicals associated with the NO_x emissions reductions (Stevenson el al., 2022).

https://doi.org/10.5194/egusphere-2025-148
Preprint. Discussion started: 4 March 2025
© Author(s) 2025. CC BY 4.0 License.

Methane, NO_x and CO mixing ratio are related through the oxidizing capacity of the atmosphere, via the abundance of the hydroxyl (OH) radical. On one side, reductions of carbon monoxide (CO) and non-methane volatile organic compound (NMVOC) emissions increase OH levels which leads to shorter methane lifetime. On the other side, reduction in nitrogen oxide (NO_x) emissions diminishes the OH level leading to a longer methane lifetime. Our regional background rural station measurements revealed that, over the 2012-2023 period, the NOx reductions were much larger than the CO decrease and were associated with large and significant increases in baseline, median and peak methane concentrations.

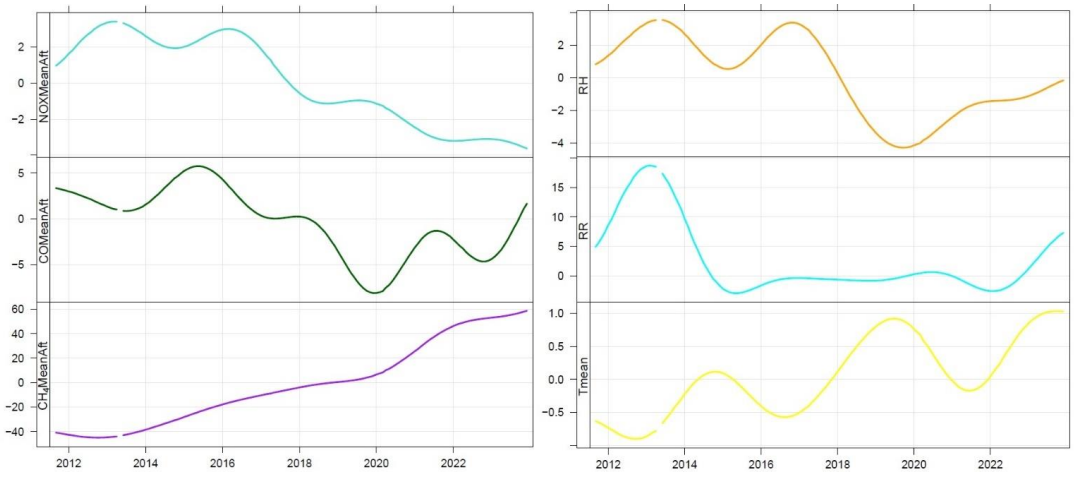

Figure 7: Long term trends computed with CCCGRV using weekly deseasonalized afternoon mean (12:00 to 16:59 UTC) NO_x (cyan upper left panel, µg m^{-3}) afternoon mean CO (green middle left panel, ppbv), afternoon mean CH_4 (purple bottom left panel, ppbv) and relative humidity (orange, upper right panel, %), precipitation (light blue, middle right panel, mm) and mean temperature (yellow, bottom right panel, °C) computed over the period 2012-2023 at OPE.

The long-term variations of the different parameters recorded at OPE over the 2012-2023 period are clearly related to different phenomena. While different processes and causes (i.e., global warming, traffic emissions reductions, agricultural and wetland methane emission increases, atmospheric circulation variations and solar activity changes) may be involved in the long-term trends as they interplay in the climate system, their impacts are quite different depending on the parameter. In the following we are thus focusing on the intra-seasonal variations, leaving apart seasonal cycles and long-term trends. We estimated the residual weekly anomalies and analyzed their relationships using cross-correlation. Figures S9 and S10 show the weekly anomalies of mean afternoon (12:00 to 16:59 UTC) O_3, NO_x, CO, CH_4 as well as ^{7}Be, ^{22}Na and the $^{7}Be/^{22}Na$ ratio and some meteorological parameters.

3.3 Weekly anomalies

After having examined the mean annual cycle and the long-term trends of surface ozone and related compounds as well as key meteorological parameters, we focused on the analysis of the weekly residuals. We computed the cross-correlations between the different compounds/parameters and looked at their seasonal evolution. Figure 8 shows the cross-correlation of the different compounds/parameters describing mean afternoon, peak or baseline ozone anomalies and several meteorological parameters associated anomalies on an annual basis. The table S3 presents the full correlation table for the different parameter's weekly anomalies.

On an annual basis, Ozone (mean afternoon, peak and baseline) residuals were significantly correlated with temperature, ^{7}Be and ^{22}Na and afternoon BLH. Ozone baseline anomalies were also significantly anti-correlated with CH_4, NO_x and CO anomalies. ^{7}Be and ^{22}Na were also significantly anti-correlated with RH anomalies on an annual basis which was strongly correlated with solar radiation anomalies.

https://doi.org/10.5194/egusphere-2025-148
Preprint. Discussion started: 4 March 2025
© Author(s) 2025. CC BY 4.0 License.

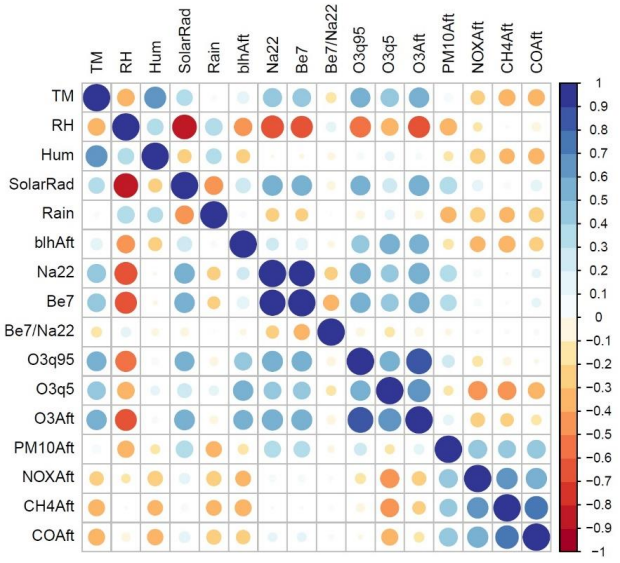

Figure 8: Cross-Correlation matrix computed using weekly residuals of temperature (TM), Relative Humidity (RH), Specific Humidity (Hum), solar radiation, rainfall, mean afternoon BLH, ^{22}Na (Na22), ^{7}Be (Be7), ^{40}K (K40), O_3 peak event (O3q95), O_3 baseline (O3q5), and afternoon mean O_3 (O3Aft), PM10 (PM10Aft), NO_x(NOXAft), CH_4 (CH4Aft) and CO (COAft) over the period 2012-2023 at OPE. The color scale indicates the value of the correlation coefficient, r.

The monthly mean correlations of several parameters (mean Temperature, RH, mean solar radiation, ^{7}Be, mean afternoon PM10, NO_x, CH_4 and CO) with mean afternoon O_3 anomalies revealed two contrasting periods (Figures S11 and S12), from November to February and from April to September. We broke down the correlation analysis into those two different periods to highlight the different residuals cross-correlations behaviors. The left panel of Figure 9 shows the cross-correlation for the period AMJJAS and the right panel shows the same correlation matrix for the period NDJF. March and October are not further considered as they seem to be transitional periods between the two contrasted seasonal regimes (Figures S11 and S12).

From November to February (right panel of Figure 9) the weekly afternoon O_3 anomalies are only weakly or not correlated with temperature (0.45), humidity (-0.24), solar radiation (0) or STT tracers (0.2) but are strongly anti-correlated with NO_x (-0.7), CH_4 (-0.8) and CO (-0.7) and are correlated with the mixing layer height anomalies (0.65). On the opposite, from April to September, the weekly afternoon O_3 anomalies are correlated with solar radiation (0.67), temperature (0.63) and with the STT tracers (0.75), anti-correlated with relative humidity (-0.7) but they are not correlated with the NO_x (0.14), CH_4 (0.25) and CO anomalies (0.4). CO and CH_4 residuals from the trends and seasonal cycles were much stronger during the cold period (October to March) than during the warm period (April to September). Eastern continental air masses or stagnant situations were associated with larger residuals and large variability in winter (Conil et al., 2019). These contrasting results highlight two complementary major influences on the weekly O_3 anomalies: solar radiation and stratosphere and upper troposphere transport to the mixing layer from April to September and precursors between November and February.

https://doi.org/10.5194/egusphere-2025-148
Preprint. Discussion started: 4 March 2025
© Author(s) 2025. CC BY 4.0 License.

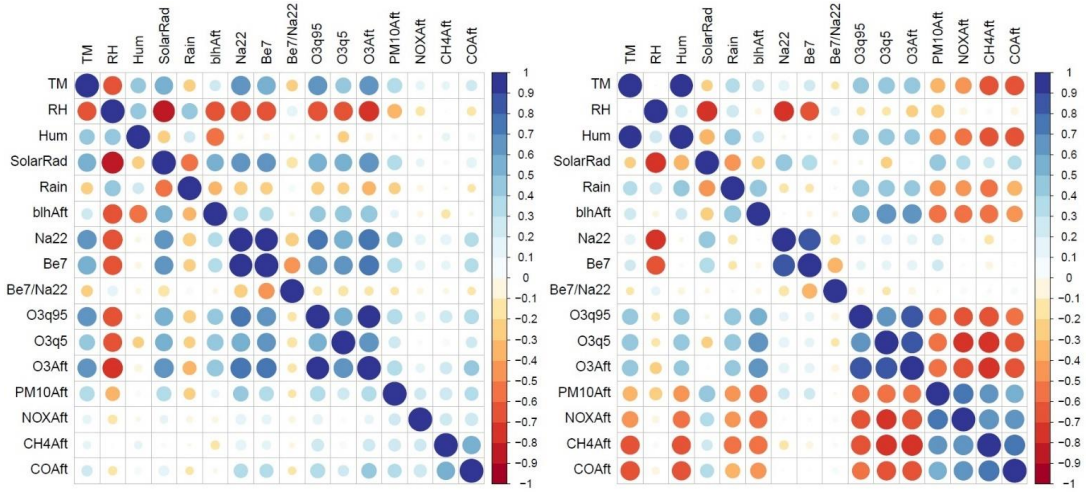

Figure 9: Cross-Correlation matrix computed for the April to September period on the left panel and for the November to February period on the right panel using weekly residuals of temperature (TM), Relative Humidity (RH), Specific Humidity (Hum), solar radiation, rainfall, mean afternoon BLH, ^{22}Na (Na22), ^{7}Be (Be7), ^{40}K (K40), O_3 peak event (O3q95), O_3 baseline (O3q5), and afternoon mean O_3 (O3Aft), PM10 (PM10Aft), NO_x(NOXAft) , CH_4 (CH4Aft) and CO (COAft) over the period 2012-2023 at OPE. The color scale indicates the value of the correlation coefficient, r.

Having identified two different periods using the correlation analysis, we then classified the ozone anomalies according to their intensity using the quantiles 10%, 25%, 40%, 60%, 75% and 90%. These seven classes were defined in order to distinguish several situations and examine their distributions:

- Large (class 1: below 10% quantile) and medium (class 2: between 10 and 25% quantiles) negative anomalies: these are situations where the O_3 concentrations are close to the background or even lower in case of titration regime occurrence.
- Situations around the typical seasonal cycle (class 4: between 40 and 60 % quantile) and with either slightly depleted O3 concentrations (class 3: between 25 and 40 % quantile) or slightly positive anomalies (class 5 : between 60 and 74 % quantile)
- Large and medium (class 7: above 90% quantile) and medium (class 6: between 75 and 90% quantiles) positive anomalies.

The residuals were distributed among these seven classes, the class 1 having the strongest negative anomalies, meaning a significant ozone depletion, the class 7 having the strongest positive anomalies, meaning a pollution event, while class 3/4/5 were associated with weaker (either negative or positive) anomalies or near normal conditions as can be shown on the upper left panel of Figure 10. We then displayed the associated tracer anomalies according to the different classes of ozone anomalies. Figure 10 reports the distribution of baseline q5, peak event q95, mean nighttime and mean afternoon ozone anomalies associated with the seven mean afternoon ozone classes for the two periods (NDJF and AMJJAS). The upper left panel shows the distribution of mean afternoon ozone residuals for each period. The classes are well defined according to the quantile definition, and they are looking very similar in both period excepting that the largest positive anomalies were occurring in the AMJJAS period. Similar patterns are shown for the mean nighttime anomalies (Figure 10; upper right panel). Despite a similar structure from negative to positive anomalies (i.e., going from class1 to class7), baseline and peak anomalies (Figure 10; bottom panels) showed contrasting characteristics: the NDJF period is associated with larger deviations of the baseline but weaker peak intensity while the AMJJAS period is associated with larger magnitude of peak events but smaller baseline variations.

https://doi.org/10.5194/egusphere-2025-148
Preprint. Discussion started: 4 March 2025
© Author(s) 2025. CC BY 4.0 License.

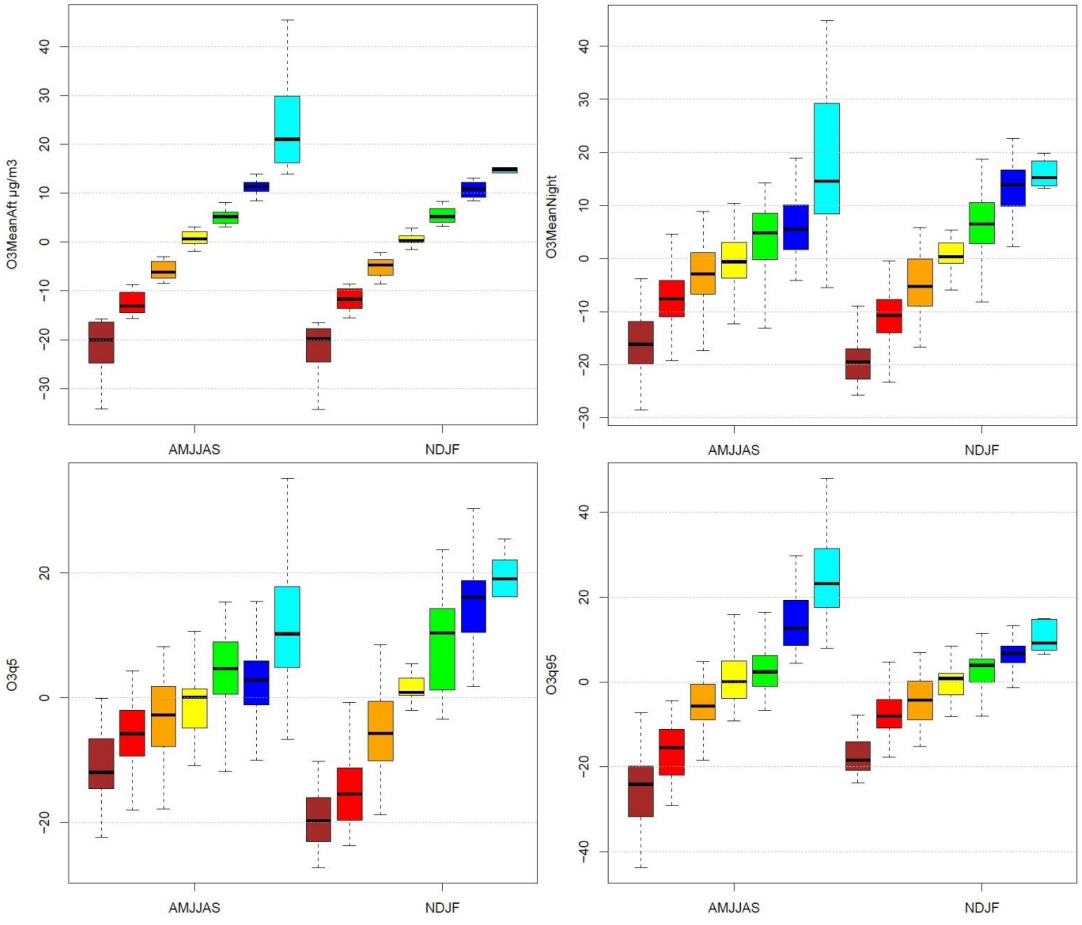

Figure 10: Boxplots of the mean afternoon ozone weekly residuals of (upper left panel, µg m^{-3}), mean nighttime (upper right panel, µg m^{-3}), baseline (q5 lower left panel, µg m^{-3}) and peak event (q95 lower right panel, µg m^{-3}) for the 7 classes of ozone anomalies over the period 2012-2023 at OPE for the AMJJAS period on the left and the NDJF period on the right of each panel. Class 1 displayed in dark red corresponds to mean afternoon O_3 anomalies below the 10% quantile, Class 2/3/4/5/6 respectively displayed in red, orange, yellow, green and blue correspond to mean afternoon O_3 anomalies between 10%, 25%, 40%, 60%, 75% and 90% quantiles, class 7 displayed in cyan corresponds to mean afternoon O_3 anomalies above the 90% quantile

The temperature, RH, solar radiation and afternoon BLH anomalies associated with the seven ozone classes are displayed on Figure 11. The distribution of temperature anomalies associated with the different O_3 classes shows that negative ozone anomalies are mostly linked with cooler situations while positive ozone anomalies are generally associated with warmer situations. But situations with warmer air and relative ozone depletion did appear as well as events with cooler air associated with an increased ozone burden as we can infer from the spread of the boxplots in class 2 and 6 for example. The distributions of RH and solar radiation anomalies among the classes are much more contrasted between the two periods. During the NDJF period, there is no clear association between ozone anomalies and RH or solar radiation residuals. But in the warm period, there are strong and significant relationships between the two. Regarding BLH, the association seems significant only during the NDJF period when larger/smaller BLH being associated with positive/negative ozone anomalies. However, the spread is quite large for each class indicating a rather nonlinear relationship implying significant roles played by other factors as depicted for the temperature.

https://doi.org/10.5194/egusphere-2025-148
Preprint. Discussion started: 4 March 2025
© Author(s) 2025. CC BY 4.0 License.

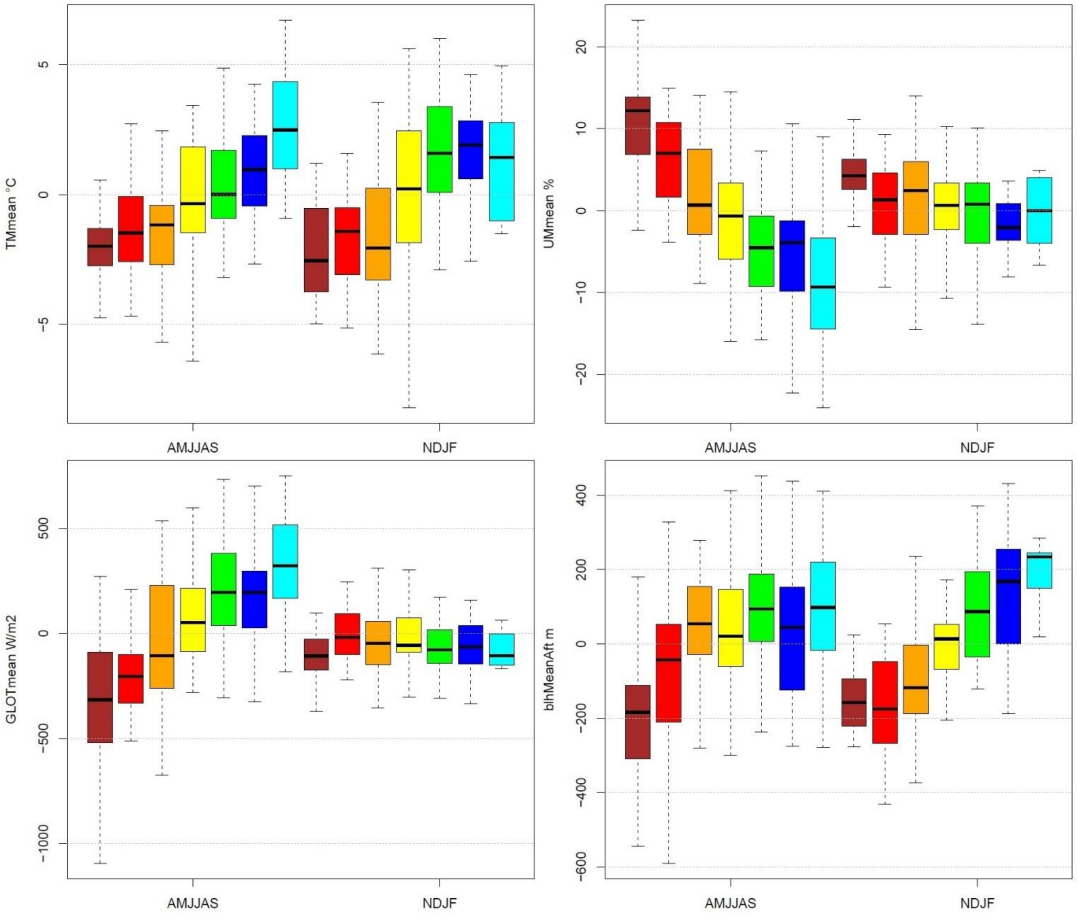

Figure 11: Boxplots of the weekly residuals of temperature (upper left panel, °C), relative humidity (upper right left panel %), solar radiation (lower left panel, W m^{-2}) and mean afternoon BLH (lower right panel, m) for the 7 classes of mean afternoon ozone anomalies over the period 2012-2023 at OPE for the AMJJAS period on the left and the NDJF period on the right of each panel. Class 1 displayed in dark red corresponds to mean afternoon O_3 anomalies below the 10% quantile, Class 2/3/4/5/6 respectively displayed in red, orange, yellow, green and blue correspond to mean afternoon O_3 anomalies between 10%, 25%, 40%, 60%, 75% and 90% quantiles, class 7 displayed in cyan corresponds to mean afternoon O_3 anomalies above the 90% quantile

Figure 12 reports the boxplots of ^{7}Be, NO_x, CH_4 and CO mean afternoon anomalies for the two periods AMJJAS and NDJF. During the NDJF period, CH_4 anomalies were strongly linked to the ozone classes, each class residuals being significantly different from the others. NO_x and CO residuals were also tightly linked to the ozone anomalies but in more complex and non-linear ways. We did not find evidence of any relation between O_3 residuals and CH_4, NO_x and CO anomalies in the AMJJAS period. On the other hand, there was no association between ^{7}Be and ozone residuals in the NDJF period. But in the AMJJAS period, the ^{7}Be residuals were significantly and almost linearly related to ozone anomalies. Similar associations were observed between ^{22}Na residuals and ozone mean afternoon anomalies. But we did not find any significant ^{7}Be/^{22}Na ratio anomalies association with ozone residuals in any of the two periods.

https://doi.org/10.5194/egusphere-2025-148
Preprint. Discussion started: 4 March 2025
© Author(s) 2025. CC BY 4.0 License.

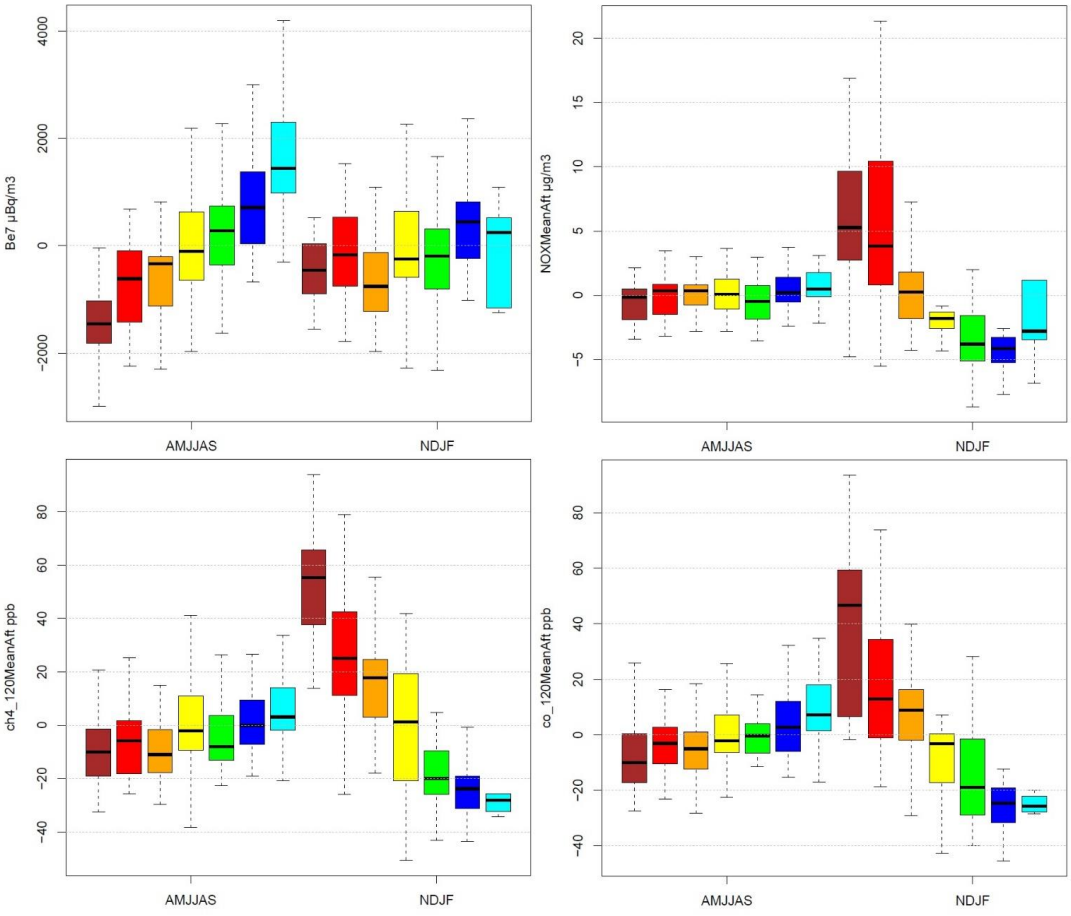

Figure 12: Boxplots of the weekly residuals of ^{7}Be (upper left panel, µBq m^{-3}), mean afternoon NO_x (upper right left panel µg m^{-3}), mean afternoon CH_4 (lower left panel, ppbv) and mean afternoon CO (lower right panel, ppbv) for the 7 classes of mean afternoon ozone anomalies over the period 2012-2023 at OPE for the AMJJAS period on the left and the NDJF period on the right of each panel. Class 1 displayed in dark red corresponds to mean afternoon O_3 anomalies below the 10% quantile, Class 2/3/4/5/6 respectively displayed in red, orange, yellow, green and blue correspond to mean afternoon O_3 anomalies between 10%, 25%, 40%, 60%, 75% and 90% quantiles, class 7 displayed in cyan corresponds to mean afternoon O_3 anomalies above the 90% quantile

The scatterplots of the relationships between O_3 anomalies and CH_4, NO_x and ^{7}Be anomalies (Figure 13 and Figure 14) confirm these seasonally contrasting relationships. During NDJF months, O_3 anomalies were almost linearly related to CH_4 and NO_x residuals but they were not associated with any distinctive pattern of ^{7}Be anomalies. During AMJJAS months, the relation with NO_x and CH_4 disappeared but the scatterplot shows a closer relationship between ^{7}Be and O_3 anomalies.

In our atmospheric dataset covering the 2012-2023 period at the OPE rural background station in Eastern France, we have shown evidence of a seasonal dependence of the weekly O_3 variability. From November to February, increases of NO_x, CO and CH_4 with anomalies ranging respectively from 5 to 10 µg/m^3, 5 to 60 ppbv and 40 to 65 ppbv, were associated with negative O_3 concentrations, with less than -20 µg m^{-3} depletion, highlighting the strong titration effect. The most discriminant parameter seems to be the CH_4 anomalies for the surface O_3 depletion in NDJF. Positive O_3 anomalies of about 10 µg m^{-3} were also associated with lower NO_x, CO and CH_4 concentrations with respectively 5 µg m^{-3} and 10 ppbv depletion.

https://doi.org/10.5194/egusphere-2025-148
Preprint. Discussion started: 4 March 2025
© Author(s) 2025. CC BY 4.0 License.

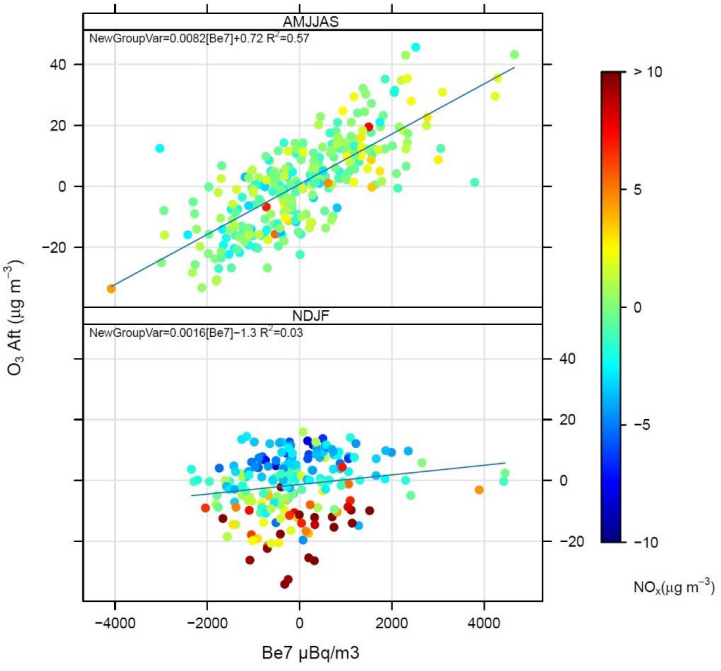

Figure 13: Scatterplots of the weekly residuals of mean afternoon O_3 vs ^7Be for the AMJJAS period (upper panel) and for the NDJF period (bottom panel). Color coding is according to mean afternoon NO_x weekly residuals. Data from 2012 to 2023 at OPE.

A linear model fit during the NDJF period indicates that a positive CH_4 anomalies of 10 ppbv is linearly associated with a mean afternoon O_3 depletion of 2.5 µg m^{-3} (with a determination coefficient R^2 of 0.57) (Figure 13). There was no evidence of temperature or solar radiation influence, but the BLH seems quite indirectly associated positively with O_3 through its relationship with the NO_X, CO and CH_4 precursors (winter lower BLH being often associated with less turbulent mixing and larger impact of regional emissions in surface concentrations). Similar results were obtained when looking at the scatterplots of afternoon CH_4 anomalies vs baseline and peak O_3 anomalies (O_3q5 and O_3q95) but with different slopes and determination coefficients R^2 (see Fig. S13 and S14). A positive CH_4 anomaly of 10 ppbv was linearly associated with baseline O_3 depletion of 3.3 µg m^{-3} (with a determination coefficient R^2 of 0.57) and a negative peak O_3 anomalies of -1.8 µg m^{-3} (with a determination coefficient R^2 of 0.44).

During the AMJJAS period, the associations between NO_X, CO and CH_4 weekly anomalies and O_3 anomalies disappeared while a stronger association with the STT proxies ^7Be and ^{22}Na was observed. Large positive afternoon O_3 anomalies (above 20 µg m^{-3}) were associated with large ^7Be anomalies (above 1,000 µBq m^{-3}). Ozone weekly variations in spring/summer are thus related to change in the vertical transport from the stratosphere and upper troposphere to the surface. A linear model fit during the AMJJAS period indicates that a positive ^7Be anomalies of 1,000 µBq m^{-3} is linearly associated with a mean afternoon O_3 enhancement of 8.2 µg/m^3 (determination coefficient R^2 0.57) The scatterplots of ^7Be anomalies vs baseline and peak O_3 anomalies (O_3q5 and O_3q95) give very similar patterns but lower determination coefficients R^2 at 0.38 and 0.5 respectively (see Fig. S15 and S16). A positive ^7Be anomalies of 1000 µBq m^{-3} is linearly associated with a baseline and peak O_3 enhancement of 4.6 µg m^{-3} and 9.4 µg m^{-3} respectively. Similar results were also obtained when looking at the mean afternoon O_3 vs ^{22}Na anomalies, a 0.1 µBq m^{-3} ^{22}Na anomalies being linearly associated with mean afternoon O_3 enhancement of 6.4 µg m^{-3} (determination coefficient R^2 0.49). There was a strong relation between ^{22}Na and ^7Be during the AMJJAS period as shown

https://doi.org/10.5194/egusphere-2025-148
Preprint. Discussion started: 4 March 2025
© Author(s) 2025. CC BY 4.0 License.

by Fig. S17, the linear fit giving a relation of 0.12 µBq m^{-3} ^{22}N with a 1,000 µBq m^{-3} ^{7}Be anomalies (determination coefficient 0.86).

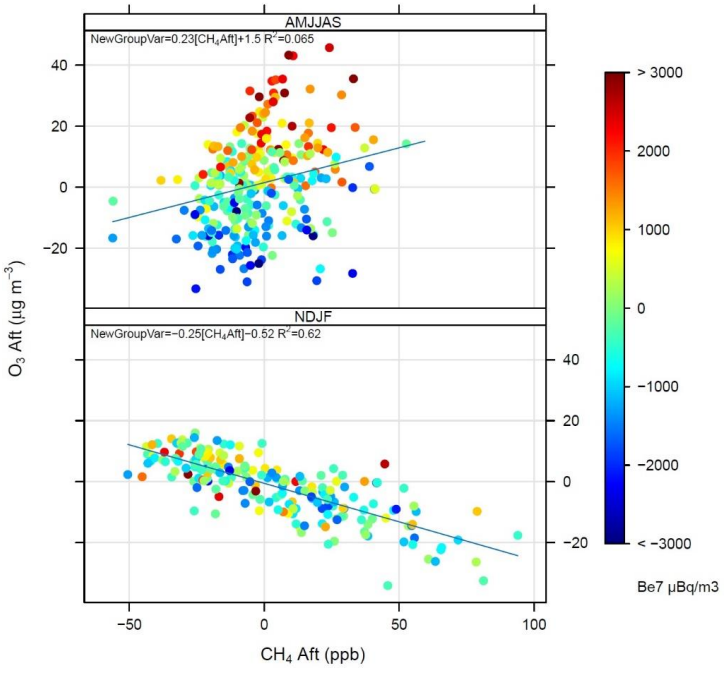

Figure 14: Scatterplots of the weekly residuals of mean afternoon O_3 vs mean afternoon CH_4 for the AMJJAS warm period (upper panel) and for the NDJF cold period (bottom panel). Color coding is according to ^{7}Be weekly residuals. Data from 2012 to 2023 at OPE.

During the AMMJAS period, 10% of the weeks considered over the 2012-2023 period experienced a mean afternoon O_3 anomaly above 20 µg m^{-3}. They were associated with baseline/peak concentrations anomalies ranging respectively from -6 / 15 µg.m^{-3} to 40/53 µg m^{-3} with median increases of 15 / 29 µg m^{-3}. The ^{7}Be and ^{22}Na anomalies ranged respectively from 415 / -0.1 µBq m^{-3} to 4,660 / 0.65 µBq m^{-3} with median increases of 1,834 / 0.206 µBq m^{-3}.

Our results show that the weekly O_3 anomalies are associated with different major drivers during the NDJF and AMMJAS periods. In NDJF, the O_3 anomalies are weakly associated with temperature, solar radiation and with STT proxies, but are closely linked with CH_4, CO and NO_X anomalies. The strongest relation was found between CH_4 and O_3 residuals, an increase of CH_4 being associated with a decrease of the O_3 anomalies. During the AMJJAS period, the relations between CH_4, CO and NO_X vanished but stronger association were noticed with STT proxies such as ^{7}Be and ^{22}Na, but also with temperature, solar radiation and relative humidity. Stratosphere and upper troposphere transport of air to the surface is associated with warming, drying and an advection of stratospheric O_3. The surface O_3 enhancement associated with ^{7}Be and ^{22}Na positive anomalies strongly suggests a direct contribution of stratospheric O_3 downdrafts. However, the link existing with warmer, drier conditions and more solar radiation indicates that this period is also favorable to local/regional photochemical production. While we were able to highlight these stratosphere and upper troposphere influence on the surface on a statistical basis from April to September, direct observations of STT events are more difficult to detect. A broad and large event occurred in June 2019 and may be used to document a STT event impact on surface conditions.

https://doi.org/10.5194/egusphere-2025-148
Preprint. Discussion started: 4 March 2025
© Author(s) 2025. CC BY 4.0 License.

3.5 The June 2019 event case study

Over the 2012-2023 period, the afternoon of June 27th of 2019 experienced the largest hourly ozone concentrations of about 200 µg m^{-3} ever recorded at the OPE regional background station. These hourly maxima were reflected in the residuals of the mean afternoon and mean nighttime ozone weekly concentrations which were also the largest (week from June 24 to June 31, 2019). During this week, the largest activity of ^{22}Na and the 6th largest value of ^{7}Be activities were also observed. Central and Western Europe experienced a significant heat wave with high ozone levels during the last days of June 2019. Many stations in Western Europe, from the Netherlands to Northern Spain and Austria, observed very high monthly means but also experienced record daily maximum temperatures. This June 2019 heat wave was associated with a "blocking" typical weather regime with a persistent ridge standing over Western Europe while land-atmosphere feedback further increased the intensity of the dynamically triggered heat (Xu et al., 2020). Vautard et al. (2020) demonstrated that these short and intense events are more frequent and higher in magnitude because of human-induced climate change. This heat wave was associated with large scale ozone peak concentrations in the eastern part of France. Massagué et al. (2024b) assessed the relative roles of transport, regional emissions and meteorology on the Barcelona area ozone dynamics during this June 2019 event. They identified several factors contributing to high ozone summer episodes: (i) initial O_3 accumulation; (ii) weekend reduction of NO_x emissions; (iii) occurrence of a foehn effect induced by a local mountain wind regime and (iv) long range transport of regional polluted air masses. Using a simplified surrogate meta model from CAMS, a source attribution method applied by Colette et al. (2022) showed the large contribution of the "natural" ozone including baseline and biogenic induced ozone and a significant traffic and industrial components whose individual effects and interactions are non-linear and can contribute positively or negatively depending on the situation. While NO_x emission reduction leads generally to ozone levels reductions in background rural areas, they can add additional ozone component by reducing ozone titration in urban areas depending on the chemical regime (Real et al., 2024). Our results suggest that STT contributed also significantly to the temperature, humidity and ozone changes during this extreme event as evidence by the high weekly average ^{7}Be and ^{22}Na values.

At OPE the air temperature (daily min, median and max) increased gradually from June 23 to June 26, 2019, in association with an increased in humidity and PM10 (Figure S18). From June 21 to June 24 the Atmospheric Pressure decreased along with the north-easterlies wind regime installation (Figure S20). On June 25, the wind regime shifted gradually to westerlies but then suddenly bounced back to easterlies on early June 26 lasting until June 30. On June 27 and 28, the temperature decreased and then increased again on June 29 and June 30 dropping back to lower nighttime minimum on July 1st (Fig. S19). During the June 27th night, a sharp increase in CH_4, NO_2, CO and O_3 baseline was observed at the OPE station (Figures S18 and S21). This nighttime increase in the O_3 baseline was followed by a rapid increase of the midday O_3 concentration associated with a fast decrease of NO_2. This 27th of June midday peak O_3 concentration was followed by a rapid drop to lower level while CH_4, CO, PM10 and absolute humidity concentrations dropped as well to their lowest value on June 28 while the temperature decreased to its lowest value over the June 21-June 30 period. In the early hours of June 30, the winds shifted, the absolute humidity rose again while PM10, CO and CH_4 increased, and ozone levels went down.

The measurements performed at that time at the OPE station offer a qualitative description of the June 2019 extreme climate and ozone event. The hourly evolution of ozone concentrations, absolute humidity and PM10 (Fig. S18), temperature, solar radiation and BLH (Fig. S19), pressure, wind speed and direction (Fig. S20) and NO_x, CH_4 and CO concentrations (Fig. S21) allow to relate the extreme ozone event and the exceptional heat wave at the end of June 2019 to a sequence of three consecutive synoptic situations. At the start of the event, the trigger was the installation of a typical ridge over Western Europe. It was accompanied by the horizontal transport of warm and dry air masses with a strong Saharan dust outbreak over the Mediterranean region and continental polluted air masses from central Europe and Benelux over the eastern part of France. Land – atmosphere processes played positive feedback to further heat up the lower atmosphere and probably increase biogenic

https://doi.org/10.5194/egusphere-2025-148
Preprint. Discussion started: 4 March 2025
© Author(s) 2025. CC BY 4.0 License.

VOC emissions (Sousa et al., 2020). At this rural location, the regional anthropogenic precursors emissions (from traffic and industrial activities) worsened the ozone conditions (Colette et al., 2022). Then a major STT event occurred, disrupting the heat wave and extreme ozone event on June 28 and 29. On those days the vertical transport component plays a key role in the temperature and ozone evolution (Xu et al., 2020, Sousa et al., 2020). The peak ozone afternoon concentration decreased but the baseline and nighttime levels stayed the same or increased. Then westerlies blown over the area bringing cooler, wetter and cleaner air, the horizontal transport component being again a key player in the ending of the event.

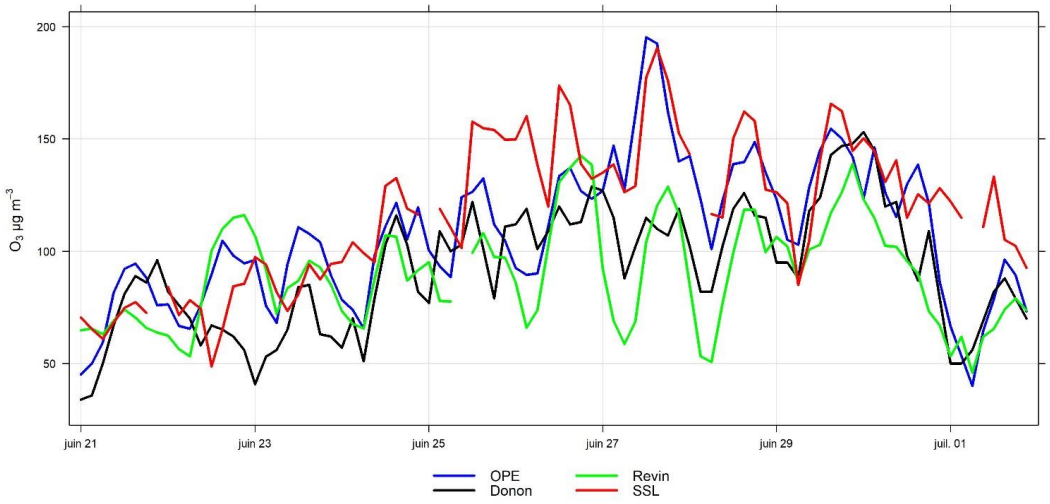

Figure 15: Hourly ozone concentration (µg m^{-3}) evolution from June 21 to July 2, 2019 at OPE (blue), Donon (black), Revin (green) and Schauinsland (SSL, red). Ozone data for Donon, Revin and Schauinsland stations were provided by EBAS.

We assessed the hourly O_3 concentration evolution at three other background stations, Revin (REV), Schauinsland (SSL) and Donon (Figure 2Figure 15) located in the northeastern part of France or in its surroundings. The Figure 15 demonstrates that, while the dominant processes in the ozone evolution have large-scale fingerprints, each station has its own characteristics and associated local variations. Evidence of such local effects is given by the difference between REV and Donon on one side and, SSL and OPE on the other side on June 27, i.e., at the time of the peak of the O_3 event and heatwave. After a steady build-up of the O_3 levels at the four stations for several days from June 20, the O_3 peaked at OPE and SSL on the afternoon on June 27 while at Donon and REV the O_3 concentrations slipped back to lower levels from the end of June 26 and thus escaping the large O_3 peak. The STT event impact on the O_3 baseline and mean levels is clearly seen at the four stations from the afternoon of June 28 to the end of June 30. The nighttime minimum concentrations increased at the four stations reaching nearly 100 µg m^{-3} early June 29 and their hourly evolution were tightly comparable reflecting the large scale of the stratospheric intrusion and its dominance over the local effects even if its different timing (as seen on the local individual atmospheric parameters) reflects the regional variations of such dynamical event.

4. Conclusion

We examined the seasonal cycles, the long-term trends and residuals of the weekly time series of median, peak and baseline values of ozone, NO_x, CO, CH_4, PM10, ^{7}Be, and ^{22}Na and their relations with the key meteorological parameters over a 12-year period in northeastern France. Surface ozone concentrations peaked in summer during the afternoon (≈ 90 µg m^{-3}) while nighttime concentrations were lower than during daytime, and peak in spring (≈ 65 µg m^{-3}). Although significant inter-annual variability has been observed, surface ozone measurements performed over the last 12 years show that the O_3 baseline at the

https://doi.org/10.5194/egusphere-2025-148
Preprint. Discussion started: 4 March 2025
© Author(s) 2025. CC BY 4.0 License.

OPE station has slightly increased and that the maximum and average values have stabilized. The decrease in NO_x and CO concentrations was contrasted by a sharp increase in CH_4 level. On the other hand, the interannual variations of ^{22}Na and ^{7}Be mirrored the sun radiation activity intensity changes, dominated by the so called 11-year solar cycle.

The intra-seasonal variability of surface ozone burden was assessed using weekly aggregated residuals. Two different periods were clearly distinguished. During the NDJF period, the nighttime and baseline ozone residual variability was larger than the afternoon and peak values. The ozone residuals were significantly related to CO, CH_4 and NO_x anomalies. Large positive anomalies of CH_4, CO and NO_x were frequently associated with air masses coming from polluted areas of Central Europe as well as lower mixing layer height and reduced dispersion and were related to significant surface ozone depletion, even more clearly depicted on the baseline and nighttime ozone anomalies. During the period extending from April to September, the surface ozone peak and mean afternoon values showed greater variability compared to baseline and nighttime values. Those ozone residuals were clearly correlated to ^{7}Be and ^{22}Na anomalies, which are fingerprints of stratospheric/upper tropospheric air mass intrusion. They were associated with drier conditions and a solar radiation increase. These weather conditions and synoptic situations also favour more active photochemical processes, suggesting that situations with a significant ozone component from stratospheric origin could frequently be associated with a larger ozone regional near surface photochemical production. Larger solar radiation, drier conditions, warmer temperatures are also associated with increased biogenic VOC emissions. Such biogenic VOC increases may significantly enhance surface ozone levels as demonstrated at many places around the world (e.g., Churkina et al, 2017; Gu et al., 2021; Ma et al., 2019; Guo et al., 2023; Zhang et al, 2023). Our results indicate that at a rural background Western European location, stratosphere/upper troposphere transport contribution to surface ozone mainly occurred in the period from April to September when ozone peaks were the largest and when natural biogenic VOC emission had the potential, with warm temperature and high solar radiation, to increase the ozone levels. During the NDJF period, when the ozone levels are lower, the ozone concentrations variations were more tightly related to anthropogenic emissions of NO_x, methane and VOC. The analysis of an exceptionally intense ozone episode that occurred in June 2019 suggests that a stratospheric intrusion was associated with a decrease of the ozone peak and an increase of the background ozone. This stratospheric transport event significantly modified the ozone budget by changing the meteorological conditions and chemical context (reducing the anthropogenic NO_X, CH_4, CO, NMVOC contributions), the vertical advection contribution being dominant over horizontal transport or photochemical processes.

Monitoring of ozone, STT tracers, NO_x, and anthropogenic and biogenic VOC is thus of primary importance in the context of an ongoing climate change that can alter any parameters in the complex nonlinear framework of the surface ozone chemistry. Further studies should also be devoted to the evaluation of global chemistry/climate models in such situation and to assess the impact of climate change under different scenario on the above-mentioned parameters and processes.

Acknowledgements

SSL, REVIN and DONON ozone data used in this were accessed from EBAS (https://ebas.nilu.no) hosted by NILU.

The authors acknowledge the work done by World Data Center SILSO, Royal Observatory of Belgium, Brussels providing free access to Sunspot Number Index.

Author contributions.

SC managed the station, did the data curation, performed most of the data analysis, interpreted the observations and prepared the manuscript. LL performed the station technical maintenance and contributed to the data curation. ML and MR contributed to the data interpretation and writing. GB designed the study and contributed to the data interpretation and to the writing. OM contributed to the data curation and to the writing. CP contributed to the data curation, data interpretation and to the writing.

Competing interests

The authors declare that they have no conflict of interest.

https://doi.org/10.5194/egusphere-2025-148
Preprint. Discussion started: 4 March 2025
© Author(s) 2025. CC BY 4.0 License.

References

Achebak H, Garatachea R, Pay MT, Jorba O, Guevara M, Pérez García-Pando C, Ballester J.: Geographic sources of ozone air pollution and mortality burden in Europe. Nat Med. 30, 1732-1738. doi: 10.1038/s41591-024-02976-x, 2024

Adame JA, I. Gutiérrez-Álvarez, P. Cristofanelli, A. Notario, J.A. Bogeat, A. López, A. Gómez, J.P. Bolívar, M. Yela.: Surface ozone trends over a 21-year period at El Arenosillo observatory (Southwestern Europe). Atmospheric Research, 269, 106048, doi:10.1016/j.atmosres.2022.106048, 2022.

Ajtić J, E. Brattich, D. Sarvan, V. Djurdjevic, M.A. Hernández-Ceballos: Factors affecting the 7Be surface concentration and its extremely high occurrences over the Scandinavian Peninsula during autumn and winter. Chemosphere, 199, 278-285, doi: 10.1016/j.chemosphere.2018.02.052, 2018.

Akritidis, D., Pozzer, A., Zanis, P., Tyrlis, E., Škerlak, B., Sprenger, M., and Lelieveld, J.: On the role of tropopause folds in summertime tropospheric ozone over the eastern Mediterranean and the Middle East, Atmos. Chem. Phys., 16, 14025–14039, https://doi.org/10.5194/acp-16-14025-2016, 2016.

Archibald A.T., J. L. Neu, Y. F. Elshorbany, O. R. Cooper, P. J. Young, H. Akiyoshi, R. A. Cox, M. Coyle, R. G. Derwent, M. Deushi, A. Finco, G. J. Frost, I. E. Galbally, G. Gerosa, C. Granier, P. T. Griffiths, R. Hossaini, L. Hu, P. Jöckel, B. Josse, M. Y. Lin, M. Mertens, O. Morgenstern, M. Naja, V. Naik, S. Oltmans, D. A. Plummer, L. E. Revell, A. Saiz-Lopez, P. Saxena, Y. M. Shin, I. Shahid, D. Shallcross, S. Tilmes, T. Trickl, T. J. Wallington, T. Wang, H. M. and Worden, G. Zeng: Tropospheric Ozone Assessment Report: A critical review of changes in the tropospheric ozone burden and budget from 1850 to 2100. Elementa: Science of the Anthropocene 2, 8, 034, https://doi.org/10.1525/elementa.2020.034. 2020

Baray, J.-L., Pointin, Y., Van Baelen, J., Lothon, M., Campistron, B., Cammas, J.-P., Masson, O., Colomb, A., Hervier, C., Bezombes, Y., Banson, S., Duroure, C., Hadad, D., and Tridon, F.: Case Study and Climatological Analysis of Upper-Tropospheric Jet Stream and Stratosphere–Troposphere Exchanges Using VHF Profilers and Radionuclide Measurements in France, J. Appl. Meteorol. Climatol., 56, 3081–3097, https://doi.org/10.1175/JAMC-D-16-0353.1, 2017.

Beekmann, M. and Vautard, R.: A modelling study of photochemical regimes over Europe: robustness and variability, Atmos. Chem. Phys., 10, 10067–10084, https://doi.org/10.5194/acp-10-10067-2010, 2010

Bell ML, Dominici F and Samet JM.: A meta-analysis of time-series studies of ozone and mortality with comparison to the national morbidity, mortality, and air pollution study. Epidemiology. 16; 436-45. doi: 10.1097/01.ede.0000165817.40152.85, 2005.

Błażej, S. and Mietelski, J.W.: Cosmogenic 22Na, 7Be and terrestrial 137Cs, 40K radionuclides in ground level air samples collected weekly in Kraków (Poland) over years 2003–2006. J Radioanal Nucl Chem, 300, 747–756, https://doi.org/10.1007/s10967-014-3049-6, 2014.

Boleti, E., Hueglin, C., Grange, S. K., Prévôt, A. S. H., and Takahama, S.: Temporal and spatial analysis of ozone concentrations in Europe based on timescale decomposition and a multi-clustering approach, Atmos. Chem. Phys., 20, 9051–9066, https://doi.org/10.5194/acp-20-9051-2020, 2020.

https://doi.org/10.5194/egusphere-2025-148
Preprint. Discussion started: 4 March 2025
© Author(s) 2025. CC BY 4.0 License.

Bourcier L, Masson O, Laj P, Pichon JM, Paulat P, Freney E, and Sellegri K.; Comparative trends and seasonal variation of ^{7}Be, ^{210}Pb and ^{137}Cs at two altitude sites in the central part of France. J Environ Radioact., 102, 294-301. doi: 10.1016/j.jenvrad.2010.12.005, 2011.

Bowman, H., Turnock, S., Bauer, S. E., Tsigaridis, K., Deushi, M., Oshima, N., O'Connor, F. M., Horowitz, L., Wu, T., Zhang, J., Kubistin, D., and Parrish, D. D.: Changes in anthropogenic precursor emissions drive shifts in the ozone seasonal cycle throughout the northern midlatitude troposphere, Atmos. Chem. Phys., 22, 3507–3524, https://doi.org/10.5194/acp-22-3507-2022, 2022

Butler, T., Lupascu, A., and Nalam, A.: Attribution of ground-level ozone to anthropogenic and natural sources of nitrogen oxides and reactive carbon in a global chemical transport model, Atmos. Chem. Phys., 20, 10707–10731, https://doi.org/10.5194/acp-20-10707-2020, 2020.

Carslaw, D. C. and K. Ropkins : openair --- an R package for air quality data analysis. Environmental Modelling & Software. 27-28, 52-61, https://doi.org/10.1016/j.envsoft.2011.09.008, 2012.

Cheesman, A.W., Brown, F., Artaxo, P., Farha, M., Folberth G., Hayes F., Heinrich V., Hill T., Mercado L., Oliver R., O'Sullivan M., Uddling J., Cernusak L. and Sitch, S.: Reduced productivity and carbon drawdown of tropical forests from ground-level ozone exposure. Nat. Geosci. 17, 1003–1007 (2024). Doi:10.1038/s41561-024-01530-1

Churkina G, Kuik F., Bonn B., Lauer A., Grote R., Tomiak K., and Butler T.M.: Effect of VOC Emissions from Vegetation on Air Quality in Berlin during a Heatwave. Environmental Science & Technology, 51, 6120-6130, doi: 10.1021/acs.est.6b06514, 2017.

Colette A, E. Real, J.M. Bertrand, and B. Raux : OZONE : ELEMENTS DE CONTEXTE SUR LES TENDANCES DE LONG TERME, LES EPISODES ET L'EFFICACITE DES MESURES DE GESTION. Note technique de l'INERIS (from https://www.lcsqa.org/fr/rapport/ozone-elements-de-contexte-sur-les-tendances-de-long-terme-les-episodes-et-lefficacite-des), 2022.

Conil, S., Helle, J., Langrene, L., Laurent, O., Delmotte, M., and Ramonet, M.: Continuous atmospheric CO2, CH4 and CO measurements at the Observatoire Pérenne de l'Environnement (OPE) station in France from 2011 to 2018, Atmos. Meas. Tech., 12, 6361–6383, https://doi.org/10.5194/amt-12-6361-2019, 2019

Cooper, O.R., D.D. Parrish, J. Ziemke, N.V. Balashov, M. Cupeiro, I.E. Galbally, S. Gilge, L. Horowitz, N.R. Jensen, J.-F. Lamarque, V. Naik, S.J. Oltmans, J. Schwab, D.T. Shindell, A.M. Thompson, V. Thouret, Y. Wang, and R.M. Zbinden: Global distribution and trends of tropospheric ozone: An observation-based review. Elementa: Science of the Anthropocene , 2, 000029, doi:10.12952/journal.elementa.000029, 2014.

Cooper, O. R., Schultz, M. G., Schröder, S., Chang, K.-L., Gaudel, A., Benítez, G. C., Cuevas, E., Fröhlich, M., Galbally, I. E., Molloy, S., Kubistin, D., Lu, X., McClure-Begley, A., Nédélec, P., O'Brien, J., Oltmans, S. J., Petropavlovskikh, I., Ries, L., Senik, I., Sjöberg, K., Solberg, S., Spain, G. T., Spangl, W., Steinbacher, M., Tarasick, D., Thouret, V., and Xu, X.: Multi-decadal surface ozone trends at globally distributed remote locations, Elementa: Science of the Anthropocene ., 8, 23, https://doi.org/10.1525/elementa.420, 2020

https://doi.org/10.5194/egusphere-2025-148
Preprint. Discussion started: 4 March 2025
© Author(s) 2025. CC BY 4.0 License.

Cristofanelli, P., P. Bonasoni, L. Tositti, U. Bonafè, F. Calzolari, F. Evangelisti, S. Sandrini, and A. Stohl: A 6-year analysis of stratospheric intrusions and their influence on ozone at Mt. Cimone (2165 m above sea level). J. Geophys. Res., 111, D03306, doi:10.1029/2005JD006553, 2006.

Cristofanelli, P., H.-E. Scheel, M. Steinbacher, M. Saliba, F. Azzopardi, R. Ellul, M. Fröhlich, L. Tositti, E. Brattich, M. Maione, F. Calzolari, R. Duchi, T.C. Landi, A. Marinoni and P. Bonasoni: Long-term surface ozone variability at Mt. Cimone WMO/GAW global station (2165 m a.s.l., Italy), Atmospheric Environment, 101, 23-33, https://doi.org/10.1016/j.atmosenv.2014.11.012, 2015.

Cristofanelli P, I. Gutiérrez, J.A. Adame, P. Bonasoni, M. Busetto, F. Calzolari, D. Putero, and F. Roccato : Interannual and seasonal variability of NOx observed at the Mt. Cimone GAW/WMO global station (2165 m a.s.l., Italy), Atmospheric Environment, 249, 118245, https://doi.org/10.1016/j.atmosenv.2021.118245, 2021.

Delaygue, G., Bekki, S., and Bard, E.: Modelling the stratospheric budget of beryllium isotopes. Tellus B: Chemical and Physical Meteorology, 67. https://doi.org/10.3402/tellusb.v67.28582, 2015.

Derwent RD, D. D., Parrish, I. E. Galbally, D. S. Stevenson, R. M. Doherty, V. Naik andR. J. Young: Uncertainties in models of tropospheric ozone based on Monte Carlo analysis: Tropospheric ozone burdens, atmospheric lifetimes and surface distributions, Atmospheric Environment, 180, 93-102, https://doi.org/10.1016/j.atmosenv.2018.02.047, 2018.

Diaz, F.M.R., Khan, M.A.H., Shallcross, B.M.A., Shallcross, E.D.G. Vogt, U. and Shallcross, D.E.: Ozone Trends in the United Kingdom over the Last 30 Years. Atmosphere, 11, 534, https://doi.org/10.3390/atmos11050534, 2020

Farman, J., Gardiner, B. and Shanklin, J.: Large losses of total ozone in Antarctica reveal seasonal ClOx/NOx interaction. Natur,e 315, 207–210, https://doi.org/10.1038/315207a0,1985

Fiore, A.M., F.J. Dentener, O. Wild, C. Cuvelier, M.G. Schultz, P. Hess, C. Textor, M. Schulz, R.M. Doherty, L.W. Horowitz, I.A. MacKenzie, M.G. Sanderson, D.T. Shindell, D.S. Stevenson, S. Szopa, R. Van Dingenen, G. Zeng, C. Atherton, D. Bergmann, I. Bey, G. Carmichael, W.J. Collins, B.N. Duncan, G. Faluvegi, G. Folberth, M. Gauss, S. Gong, D. Hauglustaine, T. Holloway, I.S.A. Isaksen, D.J. Jacob, J.E. Jonson, J.W. Kaminski, T.J. Keating, A. Lupu, E. Marmer, V. Montanaro, R.J. Park, G. Pitari, K.J. Pringle, J.A. Pyle, S. Schroeder, M.G. Vivanco, P. Wind, G. Wojcik, S. Wu, and A. Zuber: Multimodel estimates of intercontinental source-receptor relationships for ozone pollution. J. Geophys. Res., 114, D04301, doi:10.1029/2008JD010816,2009.

Fiore, A. M., Hancock, S. E., Lamarque, J.-F., Correa, G. P., Chang, K.-L., Ru, M., Cooper, O., Gaudel, A., Polvani, L. M., Sauvage, B., and Ziemke, J. R.: Understanding recent tropospheric ozone trends in the context of large internal variability: a new perspective from chemistry-climate model ensembles, Environmental Research: Climate, 1, 025008, doi:10.1088/2752-5295/ac9cc2, 2022.

Fleming, Z.L., Doherty, R.M., von Schneidemesser, E., Malley, C.S., Cooper, O.R., Pinto, J.P., Colette, A., Xu, X., Simpson, D., Schultz, M.G., Lefohn, A.S., Hamad, S., Moolla, R., Solberg, S. and Feng, Z.: Tropospheric Ozone Assessment Report: Present-day ozone distribution and trends relevant to human health. Elementa: Science of the Anthropocene, 6, 12. doi: https://doi.org/10.1525/elementa.273, 2018.

https://doi.org/10.5194/egusphere-2025-148
Preprint. Discussion started: 4 March 2025
© Author(s) 2025. CC BY 4.0 License.

Gaudel, A., Cooper, O. R., Ancellet, G., Barret, B., Boynard, A., Burrows, J. P., Clerbaux, C., Coheur, P.-F., Cuesta, J., Cuevas, E., Doniki, S., Dufour, G., Ebojie, F., Foret, G., Garcia, O., Granados-Muñoz, M. J., Hannigan, J. W., Hase, F., Hassler, B., Huang, G., Hurtmans, D., Jaffe, D., Jones, N., Kalabokas, P., Kerridge, B., Kulawik, S., Latter, B., Leblanc, T., Le Flochmoën, E., Lin, W., Liu, J., Liu, X., Mahieu, E., McClure-Begley, A., Neu, J. L., Osman, M., Palm, M., Petetin, H., Petropavlovskikh, I., Querel, R., Rahpoe, N., Rozanov, A., Schultz, M. G., Schwab, J., Siddans, R., Smale, D., Steinbacher, M., Tanimoto, H., Tarasick, D. W., Thouret, V., Thompson, A. M., Trickl, T., Weatherhead, E., Wespes, C., Worden, H. M., Vigouroux, C., Xu, X., Zeng, G., and Ziemke, J.: Tropospheric Ozone Assessment Report: Present-day distribution and trends of tropospheric ozone relevant to climate and global atmospheric chemistry model evaluation, Elementa: Science of the Anthropocene, 6, 39, https://doi.org/10.1525/elementa.291, 2018.

Gaudel, A., Cooper, O. R., Chang, K.-L., Bourgeois, I., Ziemke, J. R., Strode, S. A., Oman, L. D., Sellitto, P., Nédélec, P., Blot, R., Thouret, V., and Granier, C.: Aircraft observations since the 1990s reveal increases of tropospheric ozone at multiple locations across the Northern Hemisphere, Sci. Adv., 6, eaba8272, https://doi.org/10.1126/sciadv.aba8272, 2020.

Gaudel, A., Bourgeois, I., Li, M., Chang, K.-L., Ziemke, J., Sauvage, B., Stauffer, R. M., Thompson, A. M., Kollonige, D. E., Smith, N., Hubert, D., Keppens, A., Cuesta, J., Heue, K.-P., Veefkind, P., Aikin, K., Peischl, J., Thompson, C. R., Ryerson, T. B., Frost, G. J., McDonald, B. C., and Cooper, O. R.: Tropical tropospheric ozone distribution and trends from in situ and satellite data, Atmos. Chem. Phys., 24, 9975–10000, https://doi.org/10.5194/acp-24-9975-2024, 2024

Gilge, S., Plass-Duelmer, C., Fricke, W., Kaiser, A., Ries, L., Buchmann, B., and Steinbacher, M.: Ozone, carbon monoxide and nitrogen oxides time series at four alpine GAW mountain stations in central Europe, Atmos. Chem. Phys., 10, 12295–12316, https://doi.org/10.5194/acp-10-12295-2010, 2010

Gu S, Guenther A and Faiola C.: Effects of Anthropogenic and Biogenic Volatile Organic Compounds on Los Angeles Air Quality. Environ Sci Technol., 55, 12191-12201. doi: 10.1021/acs.est.1c01481, 2021.

Hernández-Ceballos MA, G. Cinelli, M. Marín Ferrer, T. Tollefsen, L. De Felice, E. Nweke, P.V. Tognoli, S. Vanzo, and M. De Cort : A climatology of 7Be in surface air in European Union, Journal of Environmental Radioactivity, 141, https://doi.org/10.1016/j.jenvrad.2014.12.003, 2015.

Hernández-Ceballos MA, G. Cinelli, T. Tollefsen, and M. Marín-Ferrer: Identification of airborne radioactive spatial patterns in urope – Feasibility study using Beryllium-7, Journal of Environmental Radioactivity, 155–156, https://doi.org/10.1016/j.jenvrad.2016.02.006, 2016.

Hernández-Ceballos M.A., E. Brattic and J. Ajtić: Airflow and teleconnection patterns driving the spatial and temporal variability of high 7Be air concentrations in Europe, Chemosphere, 303, https://doi.org/10.1016/j.chemosphere.2022.135194, 2022.

Holton, J. R., P. H. Haynes, M. E. McIntyre, A. R. Douglass, R. B. Rood, and L. Pfister: Stratosphere-troposphere exchange, Rev. Geophys., 33(4), 403–439, doi:10.1029/95RG02097, 1995.

https://doi.org/10.5194/egusphere-2025-148
Preprint. Discussion started: 4 March 2025
© Author(s) 2025. CC BY 4.0 License.

IPCC, 2021: Climate Change 2021: The Physical Science Basis. Contribution of Working Group I to the Sixth Assessment Report of the Intergovernmental Panel on Climate Change[Masson-Delmotte, V., P. Zhai, A. Pirani, S.L. Connors, C. Péan, S. Berger, N. Caud, Y. Chen, L. Goldfarb, M.I. Gomis, M. Huang, K. Leitzell, E. Lonnoy, J.B.R. Matthews, T.K. Maycock, T. Waterfield, O. Yelekçi, R. Yu, and B. Zhou (eds.)]. Cambridge University Press, Cambridge, United Kingdom and New York, NY, USA,

Kalabokas, P., Jensen, N. R., Roveri, M., Hjorth, J., Eremenko, M., Cuesta, J., Dufour, G., Foret, G., and Beekmann, M.: A study of the influence of tropospheric subsidence on spring and summer surface ozone concentrations at the JRC Ispra station in northern Italy, Atmos. Chem. Phys., 20, 1861–1885, https://doi.org/10.5194/acp-20-1861-2020, 2020

Krupa, S. V. and Manning, W. J.: Atmospheric ozone: Formation and effects on vegetation, Environ. follut. 50, 101-137, doi: 10.1016/0269-7491(88)90187-x, 1988

Thoning, K.W., P.P. Tans, and W.D. Komhyr: Atmospheric carbon dioxide at Mauna Loa Observatory, 2. Analysis of the NOAA/GMCC data, 1974 1985., Journal of Geophysical Research: Atmospheres, 94, 8549–8565, doi:10.1029/JD09iD06p08549, 1989

Kuang, S., Newchurch, M. J., Johnson, M. S., Wang, L., Burris, J. F., Pierce, R. B., Eloranta, E. W., Pollack, I. W., Graus, M., de Gouw, J., Warneke, C., Ryerson, T. B., Markovic, M. Z., Holloway, J. S., Pour-Biazar, A., Huang, G., Liu, X., and Feng, N.: Summertime tropospheric ozone enhancement associated with a cold front passage due to stratosphere-to-troposphere transport and biomass burning: Simultaneous ground-based lidar and airborne measurements, J. Geophys. Res., 122, 1293–1311, doi:10.1002/2016JD026078, 2017.

Lefohn AS, Lawrence JA and Kohut RJ: A comparison of indices that describe the relationship between exposure to ozone and reduction in the yield of agricultural crops. Atmos Environ, 22, 1229–1240, doi: 10.1016/0004-6981(88)90353-8, 1988.

Leppänen A and Poluianov S.: The impact of different atmospheric phenomena to cosmogenic 22Na/7Be ratio, Journal of Atmospheric and Solar-Terrestrial Physics, 236, 105918, https://doi.org/10.1016/j.jastp.2022.105918, 2022.

Lin, M., Horowitz, L. W., Payton, R., Fiore, A. M., and Tonnesen, G.: US surface ozone trends and extremes from 1980 to 2014: quantifying the roles of rising Asian emissions, domestic controls, wildfires, and climate, Atmos. Chem. Phys., 17, 2943–2970, https://doi.org/10.5194/acp-17-2943-2017, 2017.

Logan, J. A.: An analysis of ozonesonde data for the troposphere: Recommendations for testing 3-D models and development of a gridded climatology for tropospheric ozone, J. Geophys. Res., 104, 16115–16149, doi:10.1029/1998JD100096, 1999.

Lu, X., Zhang, L. and Shen, L.: Meteorology and Climate Influences on Tropospheric Ozone: a Review of Natural Sources, Chemistry, and Transport Patterns. Curr Pollution Rep,5, 238–260 https://doi.org/10.1007/s40726-019-00118-3, 2019.

Luo, Y., Zhao, T., Meng, K., Hu, J., Yang, Q., Bai, Y., Yang, K., Fu, W., Tan, C., Zhang, Y., Zhang, Y., and Li, Z.: A mechanism of stratospheric O3 intrusion into the atmospheric environment: a case study of the North China Plain, Atmos. Chem. Phys., 24, 7013–7026, https://doi.org/10.5194/acp-24-7013-2024, 2024.

https://doi.org/10.5194/egusphere-2025-148
Preprint. Discussion started: 4 March 2025
© Author(s) 2025. CC BY 4.0 License.

Luyanas, V. Y., R. Y. Yasyulyonis, D. A. Shopauskiene, and B. I. Styra: Cosmogenic 22Na, 7Be, 32P, and 33P in atmospheric dynamics research, J. Geophys. Res., 75(18), 3665–3667, doi:10.1029/JC075i018p03665, 1970.

Ma, T., Duan, F. K., He, K. B., Qin, Y., Tong, D., Geng, G. N., Liu, X. Y., Li, H., Yang, S., Ye, S. Q., Xu, B. Y., Zhang, Q., and Ma, Y. L.: Air pollution characteristics and their relationship with emissions and meteorology in the Yangtze River Delta region during 2014–2016, J. Environ. Sci., 83, 8–20, https://doi.org/10.1016/j.jes.2019.02.031, 2019.

Macé: Guide de validation des données de mesures automatiques (in french) https://www.lcsqa.org/fr/rapport/2015/ineris-lne-mines-douai/guide-methodologique-validation-donnees-mesures-automatiques, 2016

Massagué, J., Escudero, M., Alastuey, A., Monfort, E , Gangoiti, G. , Petetin, H. , Pérez García-Pando, C. ,and Querol, X. : Drivers of divergent trends in tropospheric ozone hotspots in Spain, 2008–2019. Air Qual Atmos Health 17, 621–639, https://doi.org/10.1007/s11869-023-01468-0, 2024a.

Massagué, J., Torre-Pascual, E., Carnerero, C., Escudero, M., Alastuey, A., Pandolfi, M., Querol, X., and Gangoiti, G.: Extreme ozone episodes in a major Mediterranean urban area, Atmos. Chem. Phys., 24, 4827–4850, https://doi.org/10.5194/acp-24-4827-2024, 2024b.

Massagué, J., Carnerero, C., Escudero, M., Baldasano, J. M., Alastuey, A., and Querol, X.: 2005–2017 ozone trends and potential benefits of local measures as deduced from air quality measurements in the north of the Barcelona metropolitan area, Atmos. Chem. Phys., 19, 7445–7465, https://doi.org/10.5194/acp-19-7445-2019, 2019.

Massagué J, Escudero, M., Alastuey, A., Mantilla E., Monfort, E , Gangoiti, G. , Petetin, H. , Pérez García-Pando, C. ,and Querol, X: Spatiotemporal variations of tropospheric ozone in Spain (2008–2019), Environment International, 176, 107961, https://doi.org/10.1016/j.envint.2023.107961, 2023.

Masson, O. , Steinhauser, G. , Zok, D. , Saunier, O. , Angelov, H. , Babić, D. , Bečková, V. , Bieringer, J. , Bruggeman, M. , Burbidge, C. I. , Conil, S. , Dalheimer, A. , De Geer, L. E. , de Vismes Ott, A. , Eleftheriadis, K. , Estier, S. , Fischer, H. , Garavaglia, M. G. , Gasco Leonarte, C. , Gorzkiewicz, K. , Hainz, D. , Hoffman, I. , Hýža, M. , Isajenko, K. , Karhunen, T. , Kastlander, J. , Katzlberger, C. , Kierepko, R. , Knetsch, G. J. , Kövendiné Kónyi, J. , Lecomte, M. , Mietelski, J. W. , Min, P. , Møller, B. , Nielsen, S. P. , Nikolic, J. , Nikolovska, L. , Penev, I. , Petrinec, B. , Povinec, P. P. , Querfeld, R. , Raimondi, O. , Ransby, D. , Ringer, W. , Romanenko, O. , Rusconi, R. , Saey, P. R. J. , Samsonov, V. , Šilobritienė, B. , Simion, E. , Söderström, C. , Šoštarić, M. , Steinkopff, T. , Steinmann, P. , Sýkora, I. , Tabachnyi, L. , Todorovic, D. , Tomankiewicz, E. , Tschiersch, J. , Tsibranski, R. , Tzortzis, M. , Ungar, K. , Vidic, A. , Weller, A. , Wershofen, H. , Zagyvai, P. , Zalewska, T. , Zapata García, D. and Zorko, B.: Airborne concentrations and chemical considerations of radioactive ruthenium from an undeclared major nuclear release in 2017 , Proceedings of the National Academy of Sciences, p. 201907571 . doi: 10.1073/pnas.1907571116, 2019.

Mayer M, Schreier SF, Spangl W, Staehle C, Trimmel H, Rieder HE: An analysis of 30 years of surface ozone concentrations in Austria: temporal evolution, changes in precursor emissions and chemical regimes, temperature dependence, and lessons for the future. Environ Sci Atmos., 2, 601-615, doi: 10.1039/d2ea00004k, 2022

https://doi.org/10.5194/egusphere-2025-148
Preprint. Discussion started: 4 March 2025
© Author(s) 2025. CC BY 4.0 License.

McHugh, K., Cummins, T. and Aherne, J.: Distribution and Long-Term Trends of Tropospheric Ozone Concentrations in Ireland. Atmosphere, 14, 569. https://doi.org/10.3390/atmos14030569, 2023.

Mills G, Hayes F, Simpson D, Emberson, L., Norris, D., Harmen, H. and Buker, P.: Evidence of widespread effects of ozone on crops and (semi-)natural vegetation in Europe (1990–2006) in relation to AOT40- and flux-based risk maps. Global Change Biology, 17: 592-613. https://doi.org/10.1111/j.1365-2486.2010.02217.x, 2011.

Monks P. S: A review of the observations and origins of the spring ozone maximum, Atmospheric Environment, 34, 3545-3561, https://doi.org/10.1016/S1352-2310(00)00129-1, 2000

Monks, P. S., Granier, C., Fuzzi, S., Stohl, A., Williams, M. L., Akimoto, H., Amann, M., Baklanov, A., Baltensperger, U., Bey, I., Blake, N., Blake, R. S., Carslaw, K., Cooper, O. R., Dentener, F., Fowler, D., Fragkou, E., Frost, G. J., Generoso, S., Ginoux, P., Grewe, V., Guenther, A., Hansson, H. C., Henne, S., Hjorth, J., Hofzumahaus, A., Huntrieser, H., Isaksen, I. S. A., Jenkin, M. E., Kaiser, J., Kanakidou, M., Klimont, Z., Kulmala, M., Laj, P., Lawrence, M. G., Lee, J. D., Liousse, C., Maione, M., McFiggans, G., Metzger, A., Mieville, A., Moussiopoulos, N., Orlando, J. J., O'Dowd, C. D., Palmer, P. I., Parrish, D. D., Petzold, A., Platt, U., Poeschl, U., Prevot, A. S. H., Reeves, C. E., Reimann, S., Rudich, Y., Sellegri, K., Steinbrecher, R., Simpson, D., ten Brink, H., Theloke, J., van der Werf, G. R., Vautard, R., Vestreng, V., Vlachokostas, C., and von Glasow, R.: Atmospheric composition change – global and regional air quality, Atmos. Environ., 43, 5268–5350, doi:10.1016/j.atmosenv.2009.08.021, 2009

Monks, P. S., Archibald, A. T., Colette, A., Cooper, O., Coyle, M., Derwent, R., Fowler, D., Granier, C., Law, K. S., Mills, G. E., Stevenson, D. S., Tarasova, O., Thouret, V., von Schneidemesser, E., Sommariva, R., Wild, O., and Williams, M. L.: Tropospheric ozone and its precursors from the urban to the global scale from air quality to short-lived climate forcer, Atmos. Chem. Phys., 15, 8889–8973, https://doi.org/10.5194/acp-15-8889-2015, 2015

Nguyen, D.-H., Lin, C., Vu, C.-T., Cheruiyot, N. K., Nguyen, M. K., Le, T. H., Lukkhasorn, W., and Bui, X.-T.: Tropospheric ozone and NOX: a review of worldwide variation and meteorological influences, Environmental Technology & Innovation, 28, 102809, https://doi.org/10.1016/j.eti.2022.102809, 2022.

Otero, N., Sillmann, J., Schnell, J. L., Rust, H., and Butler, T.: Synoptic and meteorological drivers of extreme ozone concentrations over Europe, Environ. Res. Lett., 11, 024005, https://doi.org/10.1088/1748-9326/11/2/024005, 2016.

Parrish, D. D., Law, K. S., Staehelin, J., Derwent, R., Cooper, O. R., Tanimoto, H., Volz-Thomas, A., Gilge, S., Scheel, H.-E., Steinbacher, M., and Chan, E.: Long-term changes in lower tropospheric baseline ozone concentrations at northern mid-latitudes, Atmos. Chem. Phys., 12, 11485–11504, https://doi.org/10.5194/acp-12-11485-2012, 2012.

Parrish, D. D., K. S. Law, J. Staehelin, R. Derwent, O. R. Cooper, H. Tanimoto, A. Volz-Thomas, S. Gilge, H.-E. Scheel, M. Steinbacher, and E. Chan: Lower tropospheric ozone at northern midlatitudes: Changing seasonal cycle, Geophys. Res. Lett., 40, 1631–1636, doi: 10.1002/grl.50303, 2013

Parrish, D. D., Petropavlovskikh, I., and Oltmans, S. J.: Reversal of long-term trend in baseline ozone concentrations at the North American West Coast. Geophysical Research Letters, 44, 10,675–10,681. https://doi.org/10.1002/2017GL074960, 2017.

https://doi.org/10.5194/egusphere-2025-148
Preprint. Discussion started: 4 March 2025
© Author(s) 2025. CC BY 4.0 License.

Pawlak, I., Krzyścin, J.and Jarosławski, J.: Long-Term Variability of Surface Ozone and Its Associations with NOx and Air Temperature Changes from Air Quality Monitoring at Belsk, Poland, 1995–2023. Atmosphere , 15, 960. https://doi.org/10.3390/atmos15080960, 2024

Pickers, P. A. and Manning, A. C.: Investigating bias in the application of curve fitting programs to atmospheric time series, Atmos. Meas. Tech., 8, 1469–1489, https://doi.org/10.5194/amt-8-1469-2015, 2015.

Putero, D., Cristofanelli, P., Sprenger, M., Škerlak, B., Tositti, L., and Bonasoni, P.: STEFLUX, a tool for investigating stratospheric intrusions: application to two WMO/GAW global stations, Atmos. Chem. Phys., 16, 14203–14217, https://doi.org/10.5194/acp-16-14203-2016, 2016.

Real E, A. Megaritis, A. Colette, G. Valastro and P. Messina: Atlas of ozone chemical regimes in Europe, Atmospheric Environment, 320, 120323, https://doi.org/10.1016/j.atmosenv.2023.120323, 2024.

Ruiz, D. J. and Prather, M. J.: From the middle stratosphere to the surface, using nitrous oxide to constrain the stratosphere–troposphere exchange of ozone, Atmos. Chem. Phys., 22, 2079–2093, https://doi.org/10.5194/acp-22-2079-2022, 2022.

Rodríguez-Perulero A, A. Baeza and J. Guillén: Seasonal evolution of 7,10Be and 22Na in the near surface atmosphere of Cáceres (Spain).Journal of Environmental Radioactivity, 197, https://doi.org/10.1016/j.jenvrad.2018.11.015, 2019.

Shen L. and Mickley L.J.: Seasonal prediction of US summertime ozone using statistical analysis of large scale climate patterns. Proceedings of the National Academy of Sciences, 114, 2491-2496. doi: 10.1073/pnas.1610708114, 2017

Sicard P.: Ground-level ozone over time: An observation-based global overview, Current Opinion in Environmental Science & Health, Volume 19, 100226, doi;10.1016/j.coesh.2020.100226, 2021

SILSO, World Data Center - Sunspot Number and Long-term Solar Observations, Royal Observatory of Belgium, on-line Sunspot Number catalogue: http://www.sidc.be/SILSO/2011-2023

Silva, R.C.V. and Pires, J.C.M.: Surface Ozone Pollution: Trends, Meteorological Influences, and Chemical Precursors in Portugal. Sustainability, 14, 2383. https://doi.org/10.3390/su14042383, 2022

Singh, P. , Ahmad, S. , Pandey, A. , Saxena, A. , Tiwari, C. and Mishra, A.: Cosmic Ray Associated with Coronal Index and Solar Flare Index during Solar Cycle 22 - 23. International Journal of Astronomy and Astrophysics, 7, 162-173. doi: 10.4236/ijaa.2017.73013, 2017.

Škerlak, B., Pfahl, S., Sprenger, M., and Wernli, H.: A numerical process study on the rapid transport of stratospheric air down to the surface over Western North America and the Tibetan Plateau, Atmos. Chem. Phys., 19, 6535–6549, https://doi.org/10.5194/acp-19-6535-2019, 2019

Solomon, S.: Stratospheric Ozone Depletion: A Review of Concepts and History. Reviews of Geophysics, 37:275–316, doi:10.1029/1999RG900008, 1999.

https://doi.org/10.5194/egusphere-2025-148
Preprint. Discussion started: 4 March 2025
© Author(s) 2025. CC BY 4.0 License.

Sousa, P. M., D. Barriopedro, R. García-Herrera, C. Ordóñez, P. M. M. Soares and R. M. Trigo: Distinct influences of large-scale circulation and regional feedbacks in two exceptional 2019 European heatwaves. Commun Earth Environ. 1, 48, https://doi.org/10.1038/s43247-020-00048-9; 2020.

Steinmann P, Zeller M, Beuret P, Ferreri G, Estier S: Cosmogenic 7Be and 22Na in ground level air in Switzerland (1994–2011). J Environ Radioact 124:68–73, doi: 10.1016/j.jenvrad.2013.03.012, 2013.

Stevenson, D. S., Derwent, R. G., Wild, O., and Collins, W. J.: COVID-19 lockdown emission reductions have the potential to explain over half of the coincident increase in global atmospheric methane, Atmos. Chem. Phys., 22, 14243–14252, https://doi.org/10.5194/acp-22-14243-2022, 2022.

Stohl, A., Bonasoni, P., Cristofanelli, P., Collins, W., Feichter, J., Frank, A., Forster, C., Gerasopoulos, E., Gäggeler, H., James, P., Kentarchos, T., Kromp-Kolb, H., Krüger, B., Land, C., Meloen, J., Papayannis, A., Priller, A., Seibert, P., Sprenger, M., Roelofs, G. J., Scheel, H. E., Schnabel, C., Siegmund, P., Tobler, L., Trickl, T., Wernli, H., Wirth, V., Zanis, P., and Zerefos, C.: Stratosphere-troposphere exchange: A review, and what we have learned from STACCATO, J. Geophys. Res., 108, 8516, doi:10.1029/2002JD002490, 2003.

Szopa, S, V Naik, B Adhikary, P Artaxo, T Berntsen, W D Collins, S Fuzzi, L Gallardo, A Kiendler-Scharr, Z Klimont, H Liao, N Unger, P Zanis, P Ginoux, J He, and F Paulot, et al.: Short-Lived Climate Forcers In Climate Change 2021: The Physical Science Basis. Contribution of Working Group I to the Sixth Assessment Report of the Intergovernmental Panel on Climate Change, Cambridge, United Kingdom and New York, NY, USA, Cambridge University Press, doi:10.1017/9781009157896.008817-922, 2021

Terzi, L., Wotawa, G., Schoeppner, M., Kalinowski M, Saey RJ, Steinmann P, Luan L and Staten P. W.: Radioisotopes demonstrate changes in global atmospheric circulation possibly caused by global warming. Scientific Reports 10, 10695 https://doi.org/10.1038/s41598-020-66541-5, 2020.

Trickl, T., Couret, C., Ries, L., and Vogelmann, H.: Zugspitze ozone 1970–2020: the role of stratosphere–troposphere transport, Atmos. Chem. Phys., 23, 8403–8427, https://doi.org/10.5194/acp-23-8403-2023, 2023.

Trisolino P, D. Putero, J. Arduini, S. Amendola, R. Calzolari, and P. Cristofanelli : Influence of deep stratosphere-to-troposphere transport on atmospheric carbon dioxide and methane at the Mt. Cimone WMO/GAW global station (2165 m a.s.l., Italy): A multi-year (2015–2022) investigation. Atmospheric Research; 310. https://doi.org/10.1016/j.atmosres.2024.107627, 2024.

Vautard, R., S. Szopa, M. Beekmann, L. Menut, D. A. Hauglustaine, L. Rouil, and M. Roemer: Are decadal anthropogenic emission reductions in Europe consistent with surface ozone observations? Geophys. Res. Lett., 33, L13810, doi:10.1029/2006GL026080, 2006.

Vautard, R., van Aalst M, Boucher, O., Drouin A., Haustein, K., Kreienkamp, F., van Oldenborgh, G. J., Otto, F., Ribes, A., Robin Y, Schneider M., Soubeyroux, J.M., Stott, P., Seneviratne, S.I., Vogel, M. and Wehner M..: Human contribution to the record-breaking June and July 2019 heatwaves in Western Europe. Environ. Res. Lett. 15 094077, doi: 10.1088/1748-9326/aba3d4, 2020.

https://doi.org/10.5194/egusphere-2025-148
Preprint. Discussion started: 4 March 2025
© Author(s) 2025. CC BY 4.0 License.

Vogelezang, D. H. P., and Holtslag, A. A. M.: Evaluation and model impacts of alternative boundary-layer height formulations. Boundary-Layer Meteorology, 81, 245–269. https://doi.org/10.1007/BF02430331, 1996

Wang, H., Lu, X., Jacob, D. J., Cooper, O. R., Chang, K. L., Li, K., Gao, M., Liu, Y., Sheng, B., Wu, K., Wu, T., Zhang, J., Sauvage, B., Nédélec, P., Blot, R., and Fan, S.: Global tropospheric ozone trends, attributions, and radiative impacts in 1995–2017: an integrated analysis using aircraft (IAGOS) observations, ozonesonde, and multi-decadal chemical model simulations, Atmos. Chem. Phys., 22, 13753–13782, https://doi.org/10.5194/acp-22-13753-2022, 2022.

Wang, M., and Fu, Q.: Stratosphere-troposphere exchange of air masses and ozone concentrations based on reanalyses and observations. Journal of Geophysical Research: Atmospheres, 126, https://doi.org/10.1029/2021JD035159, 2021.

Xu P, Wang L, Liu Y, Chen W, Huang P.: The record-breaking heat wave of June 2019 in Central Europe. Atmos Sci Lett.,21:e964. https://doi.org/10.1002/asl.964, 2020

Yan, Y., Lin, J., and He, C.: Ozone trends over the United States at different times of day, Atmos. Chem. Phys., 18, 1185–1202, https://doi.org/10.5194/acp-18-1185-2018, 2018.

Young, P. J., V. Naik, A. M. Fiore, A. Gaudel, J. Guo, M. Y. Lin, J. L. Neu, D. D. Parrish, H. E. Rieder, J. L. Schnell, S. Tilmes, O. Wild, L. Zhang, J. Ziemke, J. Brandt, A. Delcloo, R. M. Doherty, C. Geels, M. I. Hegglin, L. Hu, U. Im, R. Kumar, A. Luhar, L. Murray, D. Plummer, J. Rodriguez, A. Saiz-Lopez, M. G. Schultz, M. T. Woodhouse and G. Zeng: Tropospheric Ozone Assessment Report: Assessment of global-scale model performance for global and regional ozone distributions, variability, and trends. Elementa: Science of the Anthropocene, 6,10, https://doi.org/10.1525/elementa.265, 2018.

Zanis, P., Hadjinicolaou, P., Pozzer, A., Tyrlis, E., Dafka, S., Mihalopoulos, N., and Lelieveld, J.: Summertime free-tropospheric ozone pool over the eastern Mediterranean/Middle East, Atmos. Chem. Phys., 14, 115–132, https://doi.org/10.5194/acp-14-115-2014, 2014

Zhang Y, J Dai, Q Li, T Chen, J Mu, G Brasseur, T Wang and L Xue: Biogenic volatile organic compounds enhance ozone production and complicate control efforts: Insights from long-term observations in Hong Kong, Atmospheric Environment, 309, 119917, https://doi.org/10.1016/j.atmosenv.2023.119917, 2023.

Ziemke, J. R., Oman, L. D., Strode, S. A., Douglass, A. R., Olsen, M. A., McPeters, R. D., Bhartia, P. K., Froidevaux, L., Labow, G. J., Witte, J. C., Thompson, A. M., Haffner, D. P., Kramarova, N. A., Frith, S. M., Huang, L.-K., Jaross, G. R., Seftor, C. J., Deland, M. T., and Taylor, S. L.: Trends in global tropospheric ozone inferred from a composite record of TOMS/OMI/MLS/OMPS satellite measurements and the MERRA-2 GMI simulation , Atmos. Chem. Phys., 19, 3257–3269, https://doi.org/10.5194/acp-19-3257-2019, 2019.